J. Fluid Mech. (1998), *vol.* 356, *pp.* 297–326. Printed in the United Kingdom

On generalized Bragg scattering of surface waves by bottom ripples

By YUMING LIU AND DICK K. P. YUE

Department of Ocean Engineering, Massachusetts Institute of Technology, Cambridge, MA 02139, USA

(Received 20 May 1997 and in revised form 2 October 1997)

We study the generalized Bragg scattering of surface waves over a wavy bottom. We consider the problem in the general context of nonlinear wave–wave interactions, and write down and provide geometric constructions for the Bragg resonance conditions for second-order triad (class I) and third-order quartet (class II and class III) wave–bottom interactions. Class I resonance involving one bottom and two surface wave components is classical. Class II resonance manifests bottom nonlinearity (it involves two bottom and two surface wave components), and has been studied in the laboratory. Class III Bragg resonance is new and is a result of free-surface nonlinearity involving resonant interaction among one bottom and three surface wave components. The amplitude of the resonant wave is quadratic in the surface wave slope and linear in the bottom steepness, and, unlike the former two cases, the resonant wave may be either reflected or transmitted (relative to the incident waves) depending on the wave–bottom geometry. To predict the initial spatial/temporal growth of the Bragg resonant wave for these resonances, we also provide the regular perturbation solution up to third order. To confirm these predictions and to obtain an efficient computational tool for general wave–bottom problems with resonant interactions, we extend and develop a powerful high-order spectral method originally developed for nonlinear wave–wave and wave–body interactions. The efficacy of the method is illustrated in high-order Bragg resonance computations in two and three dimensions. These results compare well with existing experiments and perturbation theory for the known class I and class II Bragg resonance cases, and obtain and elucidate the new class III resonance. It is shown that under realistic conditions with moderate to small surface and bottom steepnesses, the amplitudes of third-order class II and class III Bragg resonant waves can be comparable in magnitude to those resulting from class I interactions and appreciable relative to the incident wave.

1. Introduction

When an incident wave travels over and interacts with non-uniform bottom depth, the wave is modified and may be partially reflected, although for mild bottom variations the reflection is in general weak. When the bottom contains periodic undulations and the incident wave and bottom ripple wavenumbers satisfy so-called Bragg conditions, however, the Bragg scattered wave becomes resonant and can be greatly amplified. Such resonant wave interactions with bottom ripples play a significant role in the evolution of nearshore surface waves. Although not yet proven, they may also be related to the development of shore-parallel bars (e.g. Heathershaw & Davies 1985).

Owing to its importance, the resonant reflection of surface waves by bottom ripples has been studied extensively in recent years. A direct perturbation analysis shows that resonant reflection occurs when the periodic bottom undulation has a wavelength half that of the incident wave (Davies 1982). This has been confirmed in laboratory experiments (Davies & Heathershaw 1984). The resonance involves the triad interaction of two surface and one bottom wave components, and the resonant wave amplitude is linear in the surface and in the bottom wave steepnesses. We denote this class I Bragg resonance. For mild incident wave and bottom slopes, reflection at or near this Bragg resonance is well predicted by perturbation theory based on multiple scales and the assumption of linearized surface waves (Mei 1985). For small surface wave slopes, class I Bragg reflection has also been obtained using the boundary-integral-equation method (BIEM) (Dalrymple & Kirby 1986) and the successive-application-matrix model (SAMM) (Miles 1967; Guazzelli, Rey & Belzons 1992; O'Hare & Davies 1993). A major drawback of these numerical schemes which employ direct discretizations of the bottom and free surfaces is the large computational effort involved in extensions to three dimensions and to inclusion of (free-surface) nonlinear effects. For the latter, Kirby (1986) recently examined nonlinear free-surface effects on the magnitude of the class I Bragg reflection based on the extended mild slope equation, but he did not study the occurrence of higher-order Bragg resonances.

For larger wave and/or bottom steepnesses, higher-order Bragg resonances resulting from nonlinear interactions among the surface and bottom wave components can be expected. For a bottom patch containing unidirectional doubly sinusoidal ripples, significant Bragg reflection at the difference of the bottom-ripple wavenumbers is observed in experiments even for relatively small ripple amplitudes (Guazzelli *et al.* 1992). This is a result of quartet resonance involving two surface and two bottom wave components. This third-order Bragg reflection is linear/quadratic in the surface wave/bottom ripple slopes respectively, and, for realistic bottom slopes, can be comparable in magnitude (but occurs at distinct frequency) to class I Bragg reflection and to the incident wave. We denote this class II Bragg resonance. Class II Bragg reflection involving nonlinear bottom interactions can in principle be predicted by BIEM and SAMM computations. An extension of Mei (1985)'s multiple scales analysis to this case in two dimensions has recently been obtained by Rey, Guazzelli & Mei (1996).

When nonlinear free-surface effects are included, a new class of Bragg resonance involving third-order quartet interactions obtains. The resonance is among three surface and one bottom wave components, and the resonant wave is now quadratic in the surface wave steepness and linear in the bottom slope. Unlike the other two cases which involve only reflection, the resonant wave can now be either reflected or transmitted (relative to the incident wave) depending on the wave–bottom geometry (see §3.3). We denote this class III Bragg resonance.

The main objectives of this work are to understand and quantify these high-order Bragg resonance effects, and to develop and demonstrate an effective computational method for general nonlinear wave–bottom (resonant) interaction problems. The boundary-value problem is stated in §2. Generalized Bragg resonance conditions are developed in §3 where we also provide geometric interpretations/constructions for the resonant (surface and bottom) waves. In §4 we obtain the regular perturbation solution for such Bragg resonances up to third order which provides the initial growth rates of the resonant waves for later comparison. The computational approach we use is an extension of the high-order spectral (HOS) method for nonlinear wave–wave and wave–body interactions (Dommermuth & Yue 1987; Liu, Dommermuth &

Yue 1992). For completeness, the formulation and implementation of this method is outlined in §5 and convergence tests are given to support the validity and accuracy of the method. Numerical results in two and three dimensions are presented and discussed in §6 for existing and new Bragg resonance cases with comparisons made to available experiments and theory for the former. We provide a short summary in §7.

2. Statement of the problem

We consider the propagation of surface waves over an undulated bottom. Let $(x, y) \equiv \boldsymbol{x}$ be the horizontal coordinates, z the vertical coordinate, $z = 0$ the mean free surface, and $z = -h + \zeta(\boldsymbol{x})$ the varying bottom position with a (constant) mean depth h. We assume the flow to be irrotational and the fluid itself homogeneous, incompressible, and inviscid.

The flow can be described by a velocity potential $\Phi(\boldsymbol{x}, z, t)$, which satisfies the Laplace equation within the fluid. On the bottom, vanishing of the normal velocity leads to

$$\Phi_z - \nabla_{\boldsymbol{x}}\zeta \cdot \nabla_{\boldsymbol{x}}\Phi = 0 \quad \text{on} \quad z = -h + \zeta(\boldsymbol{x}), \tag{2.1}$$

where $\nabla_{\boldsymbol{x}} \equiv (\partial/\partial x, \partial/\partial y)$ denotes the horizontal gradients. On the free surface, the kinematic and dynamic boundary conditions can be combined to give

$$\Phi_{tt} + g\Phi_z + 2\nabla\Phi \cdot \nabla\Phi_t + \tfrac{1}{2}\nabla\Phi \cdot \nabla(\nabla\Phi \cdot \nabla\Phi) = 0 \quad \text{on} \quad z = \eta(\boldsymbol{x}, t), \tag{2.2}$$

where g is the gravitational acceleration and the gradient operator is $\nabla \equiv (\partial/\partial x, \partial/\partial y, \partial/\partial z)$. The boundary-value problem for Φ is complete with the imposition of a radiation condition for outgoing scattered waves in the far field.

In terms of Φ, the free-surface elevation $\eta(\boldsymbol{x}, t)$ is given by

$$\eta = -\frac{1}{g}(\Phi_t + \tfrac{1}{2}\nabla\Phi \cdot \nabla\Phi) \quad \text{on} \quad z = \eta(\boldsymbol{x}, t), \tag{2.3}$$

which follows directly from the dynamic boundary condition on the free surface.

For small bottom and free-surface wave slopes, one can try a regular perturbation solution to the stated nonlinear problem. For simplicity, we assume both bottom and free-surface slopes to be measured by the same small parameter $\epsilon \ll 1$. We write Φ and η in perturbation series:

$$\Phi(\boldsymbol{x}, z, t) = \Phi^{(1)} + \Phi^{(2)} + \cdots, \quad \text{and} \quad \eta(\boldsymbol{x}, t) = \eta^{(1)} + \eta^{(2)} + \cdots, \tag{2.4}$$

where $()^{(m)}$, $m = 1, 2, \ldots$, denotes a quantity of $O(\epsilon^m)$. We then expand the bottom and free-surface boundary conditions, (2.1) and (2.2), in Taylor series with respect to the mean bottom and free-surface positions, $z = -h$ and 0, respectively. After substituting (2.4) into the Taylor expansions and collecting terms at the respective orders, we obtain a sequence of bottom and free-surface boundary conditions applied on $z = -h$ and 0 for the perturbation potentials $\Phi^{(m)}$, $m = 1, 2, \ldots$. In addition to the radiation condition, the complete boundary-value problem for $\Phi^{(m)}$, $m = 1, 2, \ldots$, can then be given in the form:

$$\left.\begin{aligned} &\nabla^2\Phi^{(m)} = 0, && -h < z < 0, \\ &\Phi_z^{(m)} = B^{(m)}(\Phi^{(1)}, \cdots, \Phi^{(m-1)}; \zeta), && z = -h, \\ &\Phi_{tt}^{(m)} + g\Phi_z^{(m)} = F^{(m)}(\Phi^{(1)}, \cdots, \Phi^{(m-1)}; \eta^{(1)}, \cdots, \eta^{(m-1)}), && z = 0, \end{aligned}\right\} \tag{2.5}$$

where $B^{(m)}$, $F^{(m)}$ are known forcing functions given in terms of lower-order quantities

and the bottom variation ζ (for B). Upon making a Taylor series expansion of (2.3) about $z = 0$, the perturbed free-surface elevation $\eta^{(m)}$, $m = 1, 2, \ldots$, is also determined in terms of the perturbation potentials $\Phi^{(\ell)}$, $\ell = 1, 2, \ldots, m$.

The sequence of boundary-value problems for $\Phi^{(m)}$, (2.5), can presumably be solved successively, starting from $m = 1$, up to any order for a wave field travelling over a given bottom topography. The procedure, however, breaks down if resonant wave–wave or wave–bottom interaction conditions obtain. For a (single) sinusoidal bottom variation, for example, the solution breaks down at $m = 2$ at discrete free-surface wavenumbers associated with (class I) Bragg resonant interactions among the surface waves and bottom undulations (Davies 1982). At such Bragg resonances, the bottom forcing $B^{(2)}$ in (2.5) becomes secular so that the associated solution for $\Phi^{(2)}$ is singular. Physically, this implies that a progressive wave is generated whose amplitude grows with time. We now consider the general conditions under which such resonances obtain.

3. Generalized Bragg conditions

The mechanism for Bragg resonances is analogous to that for nonlinear (surface) wave–wave resonant interactions in the absence of bottom undulations. Thus, general Bragg conditions can be deduced from the well-known resonance condition for nonlinear wave–wave interactions (e.g. Phillips 1960). For a wave field over uniform depth h, interactions among different wave components become resonant at order m (in wave steepness) if the wave numbers $\boldsymbol{k}_j$ and the corresponding frequencies ω_j satisfy:

$$\left.\begin{aligned} \boldsymbol{k}_1 \pm \boldsymbol{k}_2 \pm \cdots \pm \boldsymbol{k}_{m+1} &= 0 \\ \omega_1 \pm \omega_2 \pm \cdots \pm \omega_{m+1} &= 0 \end{aligned}\right\} \quad (m \geqslant 2), \tag{3.1}$$

where the same combination of signs is to be taken in both equations, and $\boldsymbol{k}_j$ and ω_j satisfy the linear dispersion relation

$$\omega_j^2 = g|\boldsymbol{k}_j| \tanh |\boldsymbol{k}_j| h. \tag{3.2}$$

Generalized Bragg resonance conditions in the presence of bottom ripples are obtained by replacing one or more of the free-surface wave components in (3.1) by periodic bottom ripple components of corresponding wavenumbers $\boldsymbol{k}_{bj}$ but with zero frequencies (since the ripples are fixed). Thus, by combining wavenumbers and frequencies of surface waves and bottom ripples, we obtain general conditions for Bragg resonances at each order, $m = 2, 3, \ldots$.

3.1. *Class I Bragg condition*

Consider two surface wave components, wavenumbers $\boldsymbol{k}_1$ and $\boldsymbol{k}_2$, propagating over a rippled horizontal bottom containing a single wavenumber $\boldsymbol{k}_b$ (analogously to surface waves, this refers to a fixed sinusoidally varying bottom with crest lines normal to $\boldsymbol{k}_b$ and with wavelength $\lambda_b = 2\pi/|\boldsymbol{k}_b|$). From (3.1), it follows that a Bragg resonance occurs at $m = 2$ (second order in the bottom/free-surface wave steepness) if

$$\left.\begin{aligned} \boldsymbol{k}_1 - \boldsymbol{k}_2 \pm \boldsymbol{k}_b &= 0, \\ \omega_1 - \omega_2 &= 0. \end{aligned}\right\} \tag{3.3}$$

Since $\omega_{1,2} > 0$, the case with the plus sign in the frequency relation (3.3) is impossible and is thus dropped. For $|\boldsymbol{k}_b| \neq 0$, the $\pm$ wavenumber relations in (3.3) cannot both

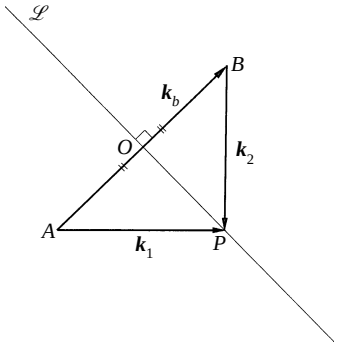

FIGURE 1. Geometric construction of the class I triad and class II quartet Bragg resonant waves.

be satisfied. As a resonance condition, it is sufficient to consider one of the signs only. For definiteness, we choose the condition for class I Bragg resonance to be

$$\left.\begin{aligned} \boldsymbol{k}_1 - \boldsymbol{k}_2 - \boldsymbol{k}_b = 0, \\ \omega_1 - \omega_2 = 0. \end{aligned}\right\} \tag{3.4}$$

From the dispersion relation (3.2), it is clear that the frequency relation in (3.4) implies that $|\boldsymbol{k}_1| = |\boldsymbol{k}_2|$. This is the classical Bragg resonance involving the triad interaction of the bottom ($\boldsymbol{k}_b$), the incident ($\boldsymbol{k}_1$ say) and the Bragg reflected wave ($\boldsymbol{k}_2$) components. The reflection is second order, being linear in both the surface and bottom wave slopes (see §4).

Given a bottom wavenumber $\boldsymbol{k}_b$, the free-surface wavenumbers $\boldsymbol{k}_1$ and $\boldsymbol{k}_2$ satisfying the class I Bragg condition (3.4) can be obtained using a simple geometric construction. The procedure is illustrated in figure 1 and consists of the following steps: (i) given the vector $\boldsymbol{k}_b = \vec{AB}$; (ii) draw its perpendicular bisector $\mathscr{L}$ which bisects AB at O; (iii) for any arbitrary point P on $\mathscr{L}$, the resonant surface wavenumbers are given by $\boldsymbol{k}_1 = \vec{AP}$, and $\boldsymbol{k}_2 = \vec{BP}$. Note that the well-known condition for two-dimensional Bragg resonance, $\boldsymbol{k}_1 = -\boldsymbol{k}_2 = \boldsymbol{k}_b/2$, is the special case when P coincides with O.

3.2. *Class II Bragg condition*

At third order ($m = 3$), quartet Bragg resonance conditions satisfying (3.1) obtain involving either two/two or three/one surface/bottom wave components. We denote these respectively class II and class III Bragg resonances. For the former, consider a doubly sinusoidal bottom containing ripples with wavenumbers $\boldsymbol{k}_{b1}$ and $\boldsymbol{k}_{b2}$. The class II Bragg resonance condition is obtained simply by replacing $\boldsymbol{k}_b$ in (3.4) by the sum or difference of $\boldsymbol{k}_{b1}$ and $\boldsymbol{k}_{b2}$:

$$\left.\begin{aligned} \boldsymbol{k}_1 - \boldsymbol{k}_2 - (\boldsymbol{k}_{b1} \pm \boldsymbol{k}_{b2}) = 0, \\ \omega_1 - \omega_2 = 0. \end{aligned}\right\} \tag{3.5}$$

The $-/+$ sign above refers to sub-/super-harmonic resonances respectively. The sub-harmonic resonance of Guazzelli *et al.* (1992) is the special two-dimensional case (all wavenumbers are in the same direction) with the $-$ sign in the wavenumber condition in (3.5). Given bottom wavenumbers $\boldsymbol{k}_{b1}$ and $\boldsymbol{k}_{b2}$, the free-surface wavenumbers $\boldsymbol{k}_1$ and $\boldsymbol{k}_2$ satisfying the class II Bragg condition (3.5) can be obtained geometrically from figure 1 by simply replacing $\boldsymbol{k}_b$ with the vector $\boldsymbol{k}_{b1} \pm \boldsymbol{k}_{b2}$.

3.3. *Class III Bragg condition*

The other wave–bottom resonance at third-order involves the quartet interaction of three surface and one bottom wave components. Consider the propagation of three surface waves, wavenumbers $\boldsymbol{k}_1, \boldsymbol{k}_2, \boldsymbol{k}_3$, over a horizontal bottom containing uniformly sinusoidal ripples, wavenumber $\boldsymbol{k}_b$. From (3.1), it follows that Bragg resonance obtains at $m = 3$ if

$$\left.\begin{aligned} \boldsymbol{k}_1 \pm \boldsymbol{k}_2 \pm \boldsymbol{k}_3 \pm \boldsymbol{k}_b = 0, \\ \omega_1 \pm \omega_2 \pm \omega_3 = 0. \end{aligned}\right\} \tag{3.6}$$

Without loss of generality, we can assume $\omega_1 \geqslant \omega_2$. It follows that $\omega_1 \pm \omega_2 + \omega_3 \neq 0$, and (3.6) can be rewritten as

$$\left.\begin{aligned} \boldsymbol{k}_1 \pm \boldsymbol{k}_2 - \boldsymbol{k}_3 \pm \boldsymbol{k}_b = 0, \\ \omega_1 \pm \omega_2 - \omega_3 = 0. \end{aligned}\right\} \tag{3.7}$$

We denote this resonance, which is quadratic in the surface wave slope and linear in the bottom slope, class III Bragg resonance.

Our interest in general is to find four surface/bottom wavenumbers such that they satisfy (3.7) to form a third-order Bragg resonance system. To do that, we apply the dispersion relation (3.2) to rewrite (3.7) as

$$\left.\begin{aligned} \boldsymbol{k}_1 \pm \boldsymbol{k}_2 - \boldsymbol{k}_3 \pm \boldsymbol{k}_b = 0, \\ (|\boldsymbol{k}_1| \tanh |\boldsymbol{k}_1|h)^{1/2} \pm (|\boldsymbol{k}_2| \tanh |\boldsymbol{k}_2|h)^{1/2} - (|\boldsymbol{k}_3| \tanh |\boldsymbol{k}_3|h)^{1/2} = 0. \end{aligned}\right\} \tag{3.8}$$

Given any two wavenumbers, then, the other two can be determined in principle from (3.8). For general finite depth, solutions to (3.8) have to be obtained numerically. To illustrate the procedure and the solution feature, we consider two special cases: (i) two of the surface wave components are identical (say, $\boldsymbol{k}_1 = \boldsymbol{k}_2$); and (ii) shallow depth, for which the dispersion relationship is simplified.

For the case of $\boldsymbol{k}_1 = \boldsymbol{k}_2$, (3.8) can be rewritten in the form

$$\left.\begin{aligned} \boldsymbol{k}_3 = 2\boldsymbol{k}_1 \pm \boldsymbol{k}_b, \\ |2\boldsymbol{k}_1 \pm \boldsymbol{k}_b| \tanh |2\boldsymbol{k}_1 \pm \boldsymbol{k}_b|h = 4|\boldsymbol{k}_1| \tanh |\boldsymbol{k}_1|h, \end{aligned}\right\} \tag{3.9}$$

where the second relation represents the fact that $\omega_3 = 2\omega_1$. Given a bottom wavenumber $\boldsymbol{k}_b$ and a mean depth h, the second relation determines the surface wavenumber $\boldsymbol{k}_1$ and then the first relation gives the surface wavenumber $\boldsymbol{k}_3$. For shallow depth ($k_b h \ll 1$), it obtains that $k_1/k_b = 1/4\cos\theta$ for the sub-harmonic case ($\boldsymbol{k}_3 = 2\boldsymbol{k}_1 - \boldsymbol{k}_b$), where θ is the angle between $\boldsymbol{k}_1$ and $\boldsymbol{k}_b$, and $k_1/k_b \to \infty$ for the super-harmonic case ($\boldsymbol{k}_3 = 2\boldsymbol{k}_1 + \boldsymbol{k}_b$). For deep depth ($k_b h \gg 1$), $k_1/k_b = [(3 + \cos^2\theta)^{1/2} \mp \cos\theta]/6$ for the sub/super-harmonic cases. Figures 2(*a*) and 2(*b*) show the solutions of $\boldsymbol{k}_1$ and $\boldsymbol{k}_3$ satisfying (3.9) for a given $\boldsymbol{k}_b$ at a number of depths for the sub- and super-harmonic cases, respectively. It is observed that for any depth, $\boldsymbol{k}_b \cdot \boldsymbol{k}_1 > 0$ and $\boldsymbol{k}_b \cdot \boldsymbol{k}_3 < 0$ for the sub-harmonic case while $\boldsymbol{k}_b \cdot \boldsymbol{k}_1 > 0$ and $\boldsymbol{k}_b \cdot \boldsymbol{k}_3 > 0$ for the super-harmonic case. This indicates that under the class III Bragg resonance, the sub/super-harmonic surface wave ($\boldsymbol{k}_3$) is always reflected/transmitted respectively relative to the incident wave ($\boldsymbol{k}_1$).

For shallow depth ($|\boldsymbol{k}_j|h \ll 1$, $j = 1, 2, 3$), we can obtain a geometric construction for the general solution. To illustrate the geometric procedure, we assume $\boldsymbol{k}_1$ and $\boldsymbol{k}_b$

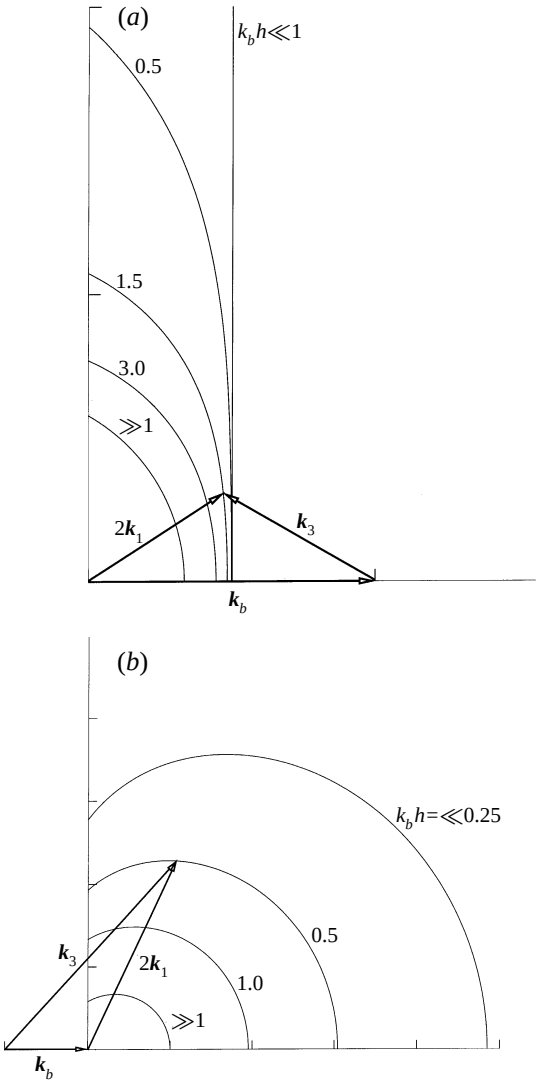

FIGURE 2. Geometric construction of the class III quartet Bragg resonant waves for $\boldsymbol{k}_2 = \boldsymbol{k}_1$ for (*a*) the sub-harmonic case: $\boldsymbol{k}_3 = 2\boldsymbol{k}_1 - \boldsymbol{k}_b$; and (*b*) the super-harmonic case: $\boldsymbol{k}_3 = 2\boldsymbol{k}_1 + \boldsymbol{k}_b$. The family of curves with different depths is obtained by satisfying the resonant condition (3.9) for a given bottom wavenumber $\boldsymbol{k}_b$ and is symmetric with respect to $\boldsymbol{k}_b$.

to be known and $\boldsymbol{k}_2$ and $\boldsymbol{k}_3$ to be determined. For shallow depth, (3.8) reduces to

$$\left.\begin{aligned} \boldsymbol{k}_3 &= \boldsymbol{k}_1 \pm \boldsymbol{k}_b \pm \boldsymbol{k}_2, \\ |\boldsymbol{k}_3| &= |\boldsymbol{k}_1| \pm |\boldsymbol{k}_2|. \end{aligned}\right\} \tag{3.10}$$

Upon substituting the first relation into the second relation, (3.10) can be expressed as

$$\left.\begin{aligned} \boldsymbol{k}_3 &= \boldsymbol{k}_1 \pm \boldsymbol{k}_b \pm \boldsymbol{k}_2, \\ |\boldsymbol{k}_1 \pm \boldsymbol{k}_b \pm \boldsymbol{k}_2| &= |\boldsymbol{k}_1| \pm |\boldsymbol{k}_2|. \end{aligned}\right\} \tag{3.11}$$

From the second equation of (3.11), it is clear that in order for $\boldsymbol{k}_2$ to exist, the $+/-$

sign should be taken before $\boldsymbol{k}_2$ and $|\boldsymbol{k}_2|$ for $|\boldsymbol{k}_1 \pm \boldsymbol{k}_b| \geqslant / \leqslant |\boldsymbol{k}_1|$. We consider the two cases, $|\boldsymbol{k}_1 \pm \boldsymbol{k}_b| \geqslant / \leqslant |\boldsymbol{k}_1|$, separately in the following.

Case A: $|\boldsymbol{k}_1 \pm \boldsymbol{k}_b| \geqslant |\boldsymbol{k}_1|$

In this case, since $|\boldsymbol{k}_3| = |\boldsymbol{k}_1| + |\boldsymbol{k}_2|$, $|\boldsymbol{k}_3| \geqslant |\boldsymbol{k}_1 + \boldsymbol{k}_2|$, (3.11) becomes

$$\left.\begin{aligned} \boldsymbol{k}_3 &= \boldsymbol{k}_1 \pm \boldsymbol{k}_b + \boldsymbol{k}_2, \\ |\boldsymbol{k}_1 \pm \boldsymbol{k}_b + \boldsymbol{k}_2| &= |\boldsymbol{k}_1| + |\boldsymbol{k}_2|. \end{aligned}\right\} \tag{3.12}$$

Given $\boldsymbol{k}_b$ and $\boldsymbol{k}_1$, the two wavenumbers $\boldsymbol{k}_2$ and $\boldsymbol{k}_3$ satisfying (3.12) can be constructed geometrically. Figure 3(*a*) illustrates the procedure for the sub-harmonic (i.e. with $-$ sign before $\boldsymbol{k}_b$) case. The steps are as follows: (i) plot the two known wavenumber vectors $\boldsymbol{k}_b = \vec{OA}$ and $\boldsymbol{k}_1 = \vec{OB}$; (ii) construct the circle $\mathscr{C}$, radius $|\boldsymbol{k}_1|$, centred at A; (iii) draw an arbitrary ray $\mathscr{L}$ from A intersecting $\mathscr{C}$ at D; (iv) find a point P on $\mathscr{L}$ such that $PB = PD$; (v) the other two resonant wavenumber vectors are given by $\boldsymbol{k}_2 = \vec{BP}$ and $\boldsymbol{k}_3 = \vec{AP}$. The complete trajectory $\mathscr{S}$ of the point P is obtained by repeating steps (iii) and (iv).

Some characteristics of the solution curve $\mathscr{S}$ can be observed from figure 3(*a*). To see these, it is helpful to: construct the normal bisector of OA, $\mathscr{L}_0$; the two tangents BE, BF to the circle $\mathscr{C}$; and extend AE and AF to form the two rays $\mathscr{L}_1$ and $\mathscr{L}_2$ (see figure 3*a*). First, $\mathscr{S}$ is tangent to $\mathscr{L}_0$ at the point G which is the solution for the case when $\boldsymbol{k}_1$ and $\boldsymbol{k}_2$ are in the same direction. The point G moves on $\mathscr{L}_0$ as the direction of $\boldsymbol{k}_1$ varies. Second, $\mathscr{S}$ lies on the same side of $\mathscr{L}_0$ as O as a result of satisfying the condition $|\boldsymbol{k}_3| \geqslant |\boldsymbol{k}_1 + \boldsymbol{k}_2|$. Third, $\mathscr{S}$ is symmetric with respect to AB and asymptotically approaches the rays $\mathscr{L}_1$ and $\mathscr{L}_2$ as $|\boldsymbol{k}_2|, |\boldsymbol{k}_3| \to \infty$.

The procedure for the super-harmonic ($+$ before $\boldsymbol{k}_b$) case is similar to the sub-harmonic case and is shown in figure 3(*b*). Unlike the sub-harmonic case (figure 3*a*), the solution curve $\mathscr{S}$ for the super-harmonic case does not intersect $\mathscr{L}_0$ and is always located on the opposite side of $\mathscr{L}_0$ relative to O.

Case B: $|\boldsymbol{k}_1 \pm \boldsymbol{k}_b| \leqslant |\boldsymbol{k}_1|$

In this case, $|\boldsymbol{k}_3| = |\boldsymbol{k}_1| - |\boldsymbol{k}_2|$, $|\boldsymbol{k}_3| \leqslant |\boldsymbol{k}_1 - \boldsymbol{k}_2|$, so that the Bragg resonance condition (3.11) can be rewritten as

$$\left.\begin{aligned} \boldsymbol{k}_3 &= \boldsymbol{k}_1 \pm \boldsymbol{k}_b - \boldsymbol{k}_2, \\ |\boldsymbol{k}_1 \pm \boldsymbol{k}_b - \boldsymbol{k}_2| &= |\boldsymbol{k}_1| - |\boldsymbol{k}_2|. \end{aligned}\right\} \tag{3.13}$$

Unlike case A, the sub-harmonic and super-harmonic cases in (3.13) cannot both be satisfied.

Given $\boldsymbol{k}_b$ and $\boldsymbol{k}_1$, the remaining wavenumbers $\boldsymbol{k}_2$ and $\boldsymbol{k}_3$ satisfying (3.13) can again be obtained geometrically. For the sub-harmonic case, $\boldsymbol{k}_3 = \boldsymbol{k}_1 - \boldsymbol{k}_2 - \boldsymbol{k}_b$, figure 4 illustrates the procedure: (i) plot the two known wavenumber vectors $\boldsymbol{k}_b = \vec{AO}$ and $\boldsymbol{k}_1 = \vec{OB}$; (ii) construct the circle $\mathscr{C}$, radius $|\boldsymbol{k}_1|$, centred at A; (iii) draw an arbitrary ray $\mathscr{L}$ from A intersecting $\mathscr{C}$ at D; (iv) find a point P on $\mathscr{L}$ such that $PB = PD$; (v) the other two resonant wavenumber vectors are given by $\boldsymbol{k}_2 = \vec{AP}$ and $\boldsymbol{k}_3 = \vec{PB}$. The complete trajectory $\mathscr{S}$ of the point P is obtained by repeating steps (iii) and (iv). The solution for the super-harmonic case, $\boldsymbol{k}_3 = \boldsymbol{k}_1 - \boldsymbol{k}_2 + \boldsymbol{k}_b$, can be constructed in a similar way and is omitted.

Unlike case A, the solution curve $\mathscr{S}$ in figure 4 is now closed (this is also true for the superharmonic case). The curve $\mathscr{S}$ is symmetric with respect to AB, is tangent to the normal bisector, $\mathscr{L}_0$, of $\boldsymbol{k}_b$, and is always located on the opposite side of $\mathscr{L}_0$ from O.

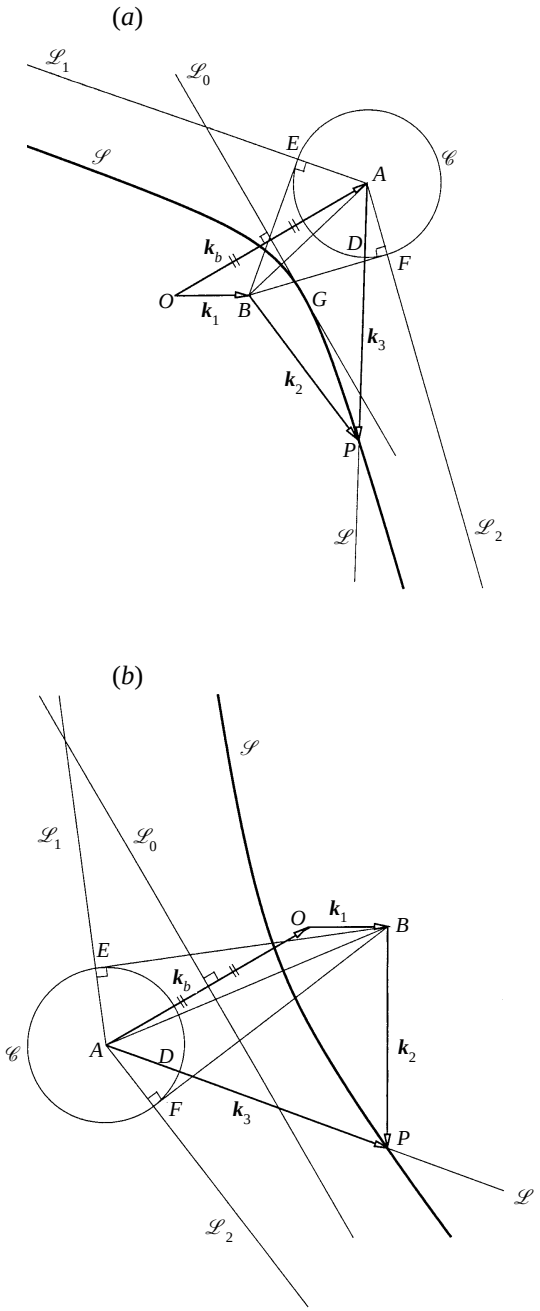

FIGURE 3. Geometric construction of the class III quartet Bragg resonant waves in the case of shallow depth for $|\boldsymbol{k}_1 \pm \boldsymbol{k}_b| \geqslant |\boldsymbol{k}_1|$ for (*a*) the sub-harmonic case: $\boldsymbol{k}_3 = \boldsymbol{k}_1 + \boldsymbol{k}_2 - \boldsymbol{k}_b$; and (*b*) the super-harmonic case: $\boldsymbol{k}_3 = \boldsymbol{k}_1 + \boldsymbol{k}_2 + \boldsymbol{k}_b$.

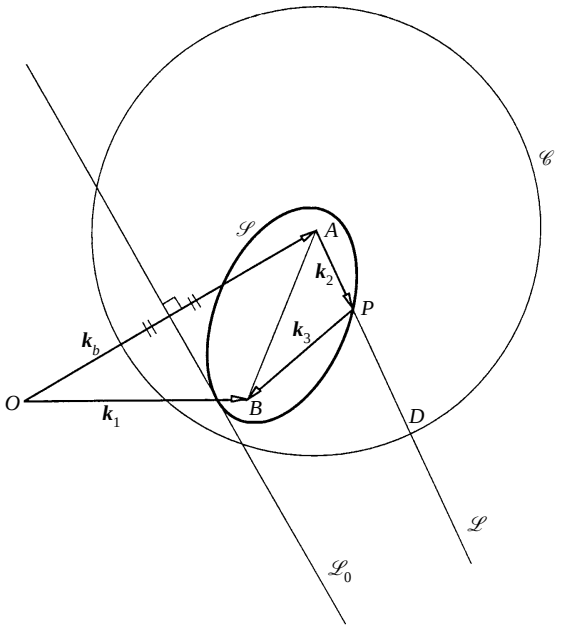

FIGURE 4. Geometric construction of the class III quartet Bragg resonant waves for $|\boldsymbol{k}_1 \pm \boldsymbol{k}_b| \leqslant |\boldsymbol{k}_1|$, for the sub-harmonic case: $\boldsymbol{k}_3 = \boldsymbol{k}_1 - \boldsymbol{k}_2 - \boldsymbol{k}_b$. The solution for the super-harmonic case, $\boldsymbol{k}_3 = \boldsymbol{k}_1 - \boldsymbol{k}_2 + \boldsymbol{k}_b$, can be contsructed similarly.

4. Perturbation solution

In this section, we solve the perturbation boundary-value problems (2.5) up to third order to obtain the solutions for the velocity potential and the free-surface elevation associated with the three classes of Bragg resonances in §3. For simplicity, we consider the special case of a single incident wave travelling on an otherwise horizontal bottom containing uniformly sinusoidal ripples (a single bottom wavenumber). As we remarked in §2, steady-state solutions to (2.5) are not meaningful under Bragg resonance conditions. In this case, the perturbation results for small time (space) provide the initial temporal (spatial) behaviour of the Bragg scattering solution.

At first order, $m = 1$, we have $B^{(1)} = F^{(1)} = 0$, and the bottom ripples do not affect the surface waves at this order. $\Phi^{(1)}$ is a homogeneous solution of (2.5) and represents, in general, a uniform propagating (or standing) wave over constant depth h. For definiteness, we choose, as incident wave, a right-going propagating wave for the first-order solution:

$$\Phi^{(1)} = \left(\frac{gA}{\omega}\right) \frac{\cosh|\boldsymbol{k}|(z+h)}{\cosh|\boldsymbol{k}|h} \sin(\boldsymbol{k}\cdot\boldsymbol{x} - \omega t), \tag{4.1}$$

$$\eta^{(1)} = A\cos(\boldsymbol{k}\cdot\boldsymbol{x} - \omega t), \tag{4.2}$$

where A is the amplitude of the incident wave with wavenumber $\boldsymbol{k} \equiv (k_x, k_y)$ and frequency ω satisfying the dispersion relation (3.2).

At second order, $m = 2$, the bottom and free-surface forcing terms are given by

$$\left.\begin{aligned} B^{(2)} &= \left[\zeta\Phi_x^{(1)}\right]_x + \left[\zeta\Phi_y^{(1)}\right]_y, && z = -h, \\ F^{(2)} &= -\eta^{(1)}\left[\Phi_{ttz}^{(1)} + g\Phi_{zz}^{(1)}\right] - 2\nabla\Phi^{(1)}\cdot\nabla\Phi_t^{(1)}, && z = 0. \end{aligned}\right\} \tag{4.3}$$

For uniformly sinusoidal ripples, the bottom variation can be expressed as

$$\zeta(\boldsymbol{x}) = d\sin(\boldsymbol{k}_b \cdot \boldsymbol{x}), \tag{4.4}$$

where d is the ripple amplitude and $\boldsymbol{k}_b$ the ripple wavenumber. Upon substituting $\Phi^{(1)}$, $\eta^{(1)}$, and ζ into (4.3), we obtain

$$\left.\begin{aligned} B^{(2)} &= \mathscr{B}^{(2)}(\boldsymbol{k}^+)\cos(\boldsymbol{k}^+ \cdot \boldsymbol{x} - \omega t) - \mathscr{B}^{(2)}(\boldsymbol{k}^-)\cos(\boldsymbol{k}^- \cdot \boldsymbol{x} - \omega t), \\ F^{(2)} &= \mathscr{F}^{(2)}\sin 2(\boldsymbol{k} \cdot \boldsymbol{x} - \omega t), \end{aligned}\right\} \tag{4.5}$$

where $\boldsymbol{k}^{\pm} = \boldsymbol{k} \pm \boldsymbol{k}_b$ and the coefficients $\mathscr{B}^{(2)}$ and $\mathscr{F}^{(2)}$ are given respectively by

$$\mathscr{B}^{(2)}(\boldsymbol{k}^{\pm}) = \frac{gAd(\boldsymbol{k} \cdot \boldsymbol{k}^{\pm})}{2\omega\cosh|\boldsymbol{k}|h} \quad \text{and} \quad \mathscr{F}^{(2)} = -\frac{3\omega^3 A^2}{2\sinh^2|\boldsymbol{k}|h}. \tag{4.6}$$

Under the class I Bragg condition (3.4), $\boldsymbol{k}^-$ and ω satisfy the dispersion relation (3.2) so that the associated forcing term in $B^{(2)}$ becomes secular. A steady-state solution is undefined in this case, and the appropriate solution for $\Phi^{(2)}$ has time-dependent amplitude and can be expressed as

$$\Phi^{(2)} = -\frac{tg\mathscr{B}^{(2)}(\boldsymbol{k}^-)\cosh|\boldsymbol{k}^-|(z+h)}{2\omega\cosh^2|\boldsymbol{k}^-|h}\sin(\boldsymbol{k}^- \cdot \boldsymbol{x} - \omega t) + \text{non-resonant terms}, \tag{4.7}$$

with the associated second-order free-surface elevation given by

$$\eta^{(2)} = -\frac{t\mathscr{B}^{(2)}(\boldsymbol{k}^-)}{2\cosh|\boldsymbol{k}^-|h}\cos(\boldsymbol{k}^- \cdot \boldsymbol{x} - \omega t) + \text{non-resonant terms}. \tag{4.8}$$

From (4.8) and (4.6), it is seen that under class I Bragg resonance, the resonant wave amplitude grows linearly in time, is linearly proportional to the free-surface and bottom wave slopes, and decreases exponentially as water depth increases.

Away from class I Bragg resonance, $\Phi^{(2)}$ is regular and its solution can be expressed as

$$\begin{aligned} \Phi^{(2)} = {} & f(\boldsymbol{k}^+, z)\cos(\boldsymbol{k}^+ \cdot \boldsymbol{x} - \omega t) - f(\boldsymbol{k}^-, z)\cos(\boldsymbol{k}^- \cdot \boldsymbol{x} - \omega t) \\ & + \left(\frac{3g|\boldsymbol{k}|A^2}{4\omega}\right)\frac{\cosh 2|\boldsymbol{k}|(z+h)}{\sinh 2|\boldsymbol{k}|h\sinh^2|\boldsymbol{k}|h}\sin 2(\boldsymbol{k} \cdot \boldsymbol{x} - \omega t), \end{aligned} \tag{4.9}$$

where the function $f(\boldsymbol{k}^{\pm}, z)$ is given by

$$f(\boldsymbol{k}^{\pm}, z) = \frac{\mathscr{B}^{(2)}(\boldsymbol{k}^{\pm})}{|\boldsymbol{k}^{\pm}|}\left[\sinh|\boldsymbol{k}^{\pm}|(z+h) - \frac{\omega^2\tanh|\boldsymbol{k}^{\pm}|h - g|\boldsymbol{k}^{\pm}|}{\omega^2 - g|\boldsymbol{k}^{\pm}|\tanh|\boldsymbol{k}^{\pm}|h}\cosh|\boldsymbol{k}^{\pm}|(z+h)\right]. \tag{4.10}$$

The second-order free-surface elevation can be obtained from

$$\eta^{(2)} = -\frac{1}{g}\Phi_t^{(2)} - \frac{1}{2g}\nabla\Phi^{(1)} \cdot \nabla\Phi^{(1)} - \frac{1}{g}\eta^{(1)}\Phi_{tz}^{(1)}, \quad z = 0. \tag{4.11}$$

Upon substituting $\Phi^{(2)}$ in (4.9), and $\Phi^{(1)}$ and $\eta^{(1)}$ into (4.11), we obtain

$$\begin{aligned} \eta^{(2)} = {} & -\frac{\omega}{g}\left[f(\boldsymbol{k}^+, 0)\sin(\boldsymbol{k}^+ \cdot \boldsymbol{x} - \omega t) - f(\boldsymbol{k}^-, 0)\sin(\boldsymbol{k}^- \cdot \boldsymbol{x} - \omega t)\right] \\ & + \left(\frac{|\boldsymbol{k}|A^2}{2}\right)\frac{2 + \cosh 2|\boldsymbol{k}|h}{\sinh 2|\boldsymbol{k}|h\tanh^2|\boldsymbol{k}|h}\cos 2(\boldsymbol{k} \cdot \boldsymbol{x} - \omega t) - \frac{|\boldsymbol{k}|A^2}{2\sinh 2|\boldsymbol{k}|h}. \end{aligned} \tag{4.12}$$

At third order, $m = 3$, the bottom and free-surface forcing terms are given by

$$B^{(3)} = \left[\zeta \Phi_x^{(2)}\right]_x + \left[\zeta \Phi_y^{(2)}\right]_y + \left[\frac{\zeta^2}{2}\Phi_x^{(1)}\right]_x + \left[\frac{\zeta^2}{2}\Phi_y^{(1)}\right]_y, \quad z = -h, \tag{4.13}$$

and

$$F^{(3)} = -\tfrac{1}{2}(\eta^{(1)})^2(\Phi_{ttzz}^{(1)} + g\Phi_{zzz}^{(1)}) - \tfrac{1}{2}\nabla\Phi^{(1)}\cdot\nabla(\nabla\Phi^{(1)}\cdot\nabla\Phi^{(1)}) - 2\eta^{(1)}\left[\nabla\Phi^{(1)}\cdot\nabla\Phi_t^{(1)}\right]_z$$
$$-\eta^{(1)}(\Phi_{ttz}^{(2)} + g\Phi_{zz}^{(2)}) - \eta^{(2)}(\Phi_{ttz}^{(1)} + g\Phi_{zz}^{(1)}) - 2\nabla\Phi^{(1)}\cdot\nabla\Phi_t^{(2)} - 2\nabla\Phi^{(2)}\cdot\nabla\Phi_t^{(1)}, \quad z = 0. \tag{4.14}$$

After substituting the first- and second-order solutions into (4.13) and (4.14), it follows that

$$B^{(3)} = \mathscr{B}_1^{(3)}(\boldsymbol{k}^+)\sin[(\boldsymbol{k}^+ + \boldsymbol{k}_b)\cdot\boldsymbol{x} - \omega t] + \mathscr{B}_1^{(3)}(\boldsymbol{k}^-)\sin[(\boldsymbol{k}^- - \boldsymbol{k}_b)\cdot\boldsymbol{x} - \omega t]$$
$$+\mathscr{B}_2^{(3)}(\boldsymbol{k}^+)\cos[(\boldsymbol{k}^+ + \boldsymbol{k})\cdot\boldsymbol{x} - 2\omega t] - \mathscr{B}_2^{(3)}(\boldsymbol{k}^-)\cos[(\boldsymbol{k}^- + \boldsymbol{k})\cdot\boldsymbol{x} - 2\omega t]$$
$$+\text{other terms}, \tag{4.15}$$

and

$$F^{(3)} = \mathscr{F}^{(3)}(\boldsymbol{k}^+)\cos[(\boldsymbol{k}^+ + \boldsymbol{k})\cdot\boldsymbol{x} - 2\omega t] - \mathscr{F}^{(3)}(\boldsymbol{k}^-)\cos[(\boldsymbol{k}^- + \boldsymbol{k})\cdot\boldsymbol{x} - 2\omega t]$$
$$+\text{other terms}, \tag{4.16}$$

where, in the above, 'other terms' represents forcing terms irrelevant to Bragg resonances. The coefficients $\mathscr{B}_1^{(3)}(\boldsymbol{k}^\pm)$, $\mathscr{B}_2^{(3)}(\boldsymbol{k}^\pm)$, and $\mathscr{F}^{(3)}(\boldsymbol{k}^\pm)$ are given respectively by

$$\mathscr{B}_1^{(3)}(\boldsymbol{k}^\pm) = \frac{gAd^2(\boldsymbol{k}\cdot\boldsymbol{k}^\pm)[\boldsymbol{k}^\pm\cdot(\boldsymbol{k}^\pm \pm \boldsymbol{k}_b)]}{4\omega|\boldsymbol{k}^\pm|\cosh|\boldsymbol{k}|h}\left(\frac{\omega^2\tanh|\boldsymbol{k}^\pm|h - g|\boldsymbol{k}^\pm|}{\omega^2 - g|\boldsymbol{k}^\pm|\tanh|\boldsymbol{k}^\pm|h}\right), \tag{4.17}$$

$$\mathscr{B}_2^{(3)}(\boldsymbol{k}^\pm) = -\frac{3g|\boldsymbol{k}|A^2d[\boldsymbol{k}\cdot(\boldsymbol{k}+\boldsymbol{k}^\pm)]}{4\omega\sinh 2|\boldsymbol{k}|h\sinh^2|\boldsymbol{k}|h}, \tag{4.18}$$

and

$$\mathscr{F}^{(3)}(\boldsymbol{k}^\pm) = \left[\frac{g\omega A^2d(\boldsymbol{k}\cdot\boldsymbol{k}^\pm)}{2|\boldsymbol{k}|\sinh 2|\boldsymbol{k}|h}\right]\frac{6|\boldsymbol{k}|^2 + (|\boldsymbol{k}^\pm|^2 + 4\boldsymbol{k}\cdot\boldsymbol{k}^\pm - 5|\boldsymbol{k}|^2)\cosh^2|\boldsymbol{k}|h}{|\boldsymbol{k}|\sinh|\boldsymbol{k}|h\cosh|\boldsymbol{k}^\pm|h - |\boldsymbol{k}^\pm|\cosh|\boldsymbol{k}|h\sinh|\boldsymbol{k}^\pm|h}. \tag{4.19}$$

If the class II Bragg resonance condition (3.5) is satisfied, the bottom forcing with wavenumber $(\boldsymbol{k}^- - \boldsymbol{k}_b)$ becomes secular. The associated solutions for the third-order velocity potential as well as the free-surface elevation are then given by

$$\Phi_1^{(3)} = -\frac{tg\mathscr{B}_1^{(3)}(\boldsymbol{k}^-)}{2\omega\cosh^2|\boldsymbol{k}^- - \boldsymbol{k}_b|h}\cosh^2|\boldsymbol{k}^- - \boldsymbol{k}_b|(z+h)\cos[(\boldsymbol{k}^- - \boldsymbol{k}_b)\cdot\boldsymbol{x} - \omega t]$$
$$+\text{non-resonant terms}, \tag{4.20}$$

and

$$\eta_1^{(3)} = \frac{t\mathscr{B}_1^{(3)}(\boldsymbol{k}^-)}{2\cosh|\boldsymbol{k}^- - \boldsymbol{k}_b|h}\sin[(\boldsymbol{k}^- - \boldsymbol{k}_b)\cdot\boldsymbol{x} - \omega t] + \text{non-resonant terms}. \tag{4.21}$$

As indicated by (4.21) and (4.17), the resonant wave amplitude for class II Bragg resonance is linear in the free-surface wave slope but quadratic in the bottom steepness.

Thus class II resonance requires the inclusion of bottom nonlinear effects but obtains without consideration of free-surface nonlinearities.

If the class III Bragg resonance condition (3.9) is satisfied, bottom and free-surface forcings with wavenumber $(\boldsymbol{k}^+ + \boldsymbol{k})$, or $(\boldsymbol{k}^- + \boldsymbol{k})$, become secular resulting in super-harmonic, or sub-harmonic, class III Bragg resonance respectively. The resonant solution for the third-order velocity potential and the free-surface elevation are then found to be

$$\Phi_2^{(3)} = \pm \frac{tg\mathscr{B}_2^{(3)}(\boldsymbol{k}^\pm) - t\mathscr{F}^{(3)}(\boldsymbol{k}^\pm)\cosh|\boldsymbol{k}^\pm + \boldsymbol{k}|h}{4\omega\cosh^2|\boldsymbol{k}^\pm + \boldsymbol{k}|h} \times \cosh|\boldsymbol{k}^\pm + \boldsymbol{k}|(z+h)\ \sin[(\boldsymbol{k}^\pm + \boldsymbol{k})\cdot\boldsymbol{x} - 2\omega t] + \text{non-resonant terms}, \quad (4.22)$$

and

$$\eta_2^{(3)} = \pm \frac{tg\mathscr{B}_2^{(3)}(\boldsymbol{k}^\pm) - t\mathscr{F}^{(3)}(\boldsymbol{k}^\pm)\cosh|\boldsymbol{k}^\pm + \boldsymbol{k}|h}{2g\cosh|\boldsymbol{k}^\pm + \boldsymbol{k}|h} \cos[(\boldsymbol{k}^\pm + \boldsymbol{k})\cdot\boldsymbol{x} - 2\omega t] + \text{non-resonant terms}. \quad (4.23)$$

Similarly to class II resonance, class III Bragg resonance occurs at third order. The resonance is, however, nonlinear (quadratic) in the free-surface wave slope but linear in bottom steepness.

We remark that the above analysis applies directly to the analogous problem of surface wave–bottom interactions over a finite distance x (measured in the direction of propagation of the resonated wave) for an unlimited time. The resonant solutions in this case can be obtained simply by replacing the time, t, in the amplitudes of (4.8), (4.21), and (4.23) by x/C_g, where C_g is the group velocity of the resonant wave. Thus, Bragg resonant wave amplitudes always grow linearly with propagation distance x and its maximum value increases linearly with the length L_0 of the bottom ripple patch. Away from resonances, the solution can be obtained by solving the associated boundary-value problem using the Fourier transform technique (Davies 1982).

One also notes that the regular perturbation solutions in this section are not valid at large time/distance under Bragg resonance conditions. To obtain uniformly valid solutions, it is generally necessary to adopt analyses based on multiple scales (e.g. Mei 1985 for class I Bragg scattering). The associated analyses for Bragg resonances involving higher orders and more surface/bottom components, however, rapidly become very long and complicated. The final results are also of limited value to the general case involving multiple (non-specific) surface and bottom wave components and resonant interactions. For these general cases of Bragg interactions, we propose an extremely efficient direct computational method based upon high-order spectral representations.

5. High-order spectral (HOS) method for wave–bottom interactions

To elucidate and validate the earlier predictions, and more importantly, to obtain a computational method useful and efficient for general nonlinear (resonant) wave–bottom interactions, we develop a highly efficient numerical solution of the problem based on the high-order spectral (HOS) method for nonlinear wave–wave (Dommermuth & Yue 1987) and wave–body (Liu *et al.* 1992) interaction problems. In this approach, the original initial-boundary-value problem associated with (2.1)

and (2.2) is solved directly and all nonlinear interactions up to an arbitrary order M in free-surface and/or bottom steepnesses are accounted for. Using orthogonal spectral expansions for the free-surface and bottom elevations, the solution converges exponentially with the number of free-surface and bottom (for general irregular topography) modes N. Furthermore, by employing fast transform techniques, the computational effort per time step is only linearly proportional to the perturbation order M and to the number of spectral modes N. The characteristics of the HOS method are thus: exponential convergence and accuracy; nearly linear computational effort; and inclusion of (arbitrary) high-order nonlinear free-surface and bottom effects.

5.1. *Mathematical formulation*

The HOS method for wave–bottom problems is an extension of and follows closely that of Dommermuth & Yue (1987) and Liu *et al.* (1992) for nonlinear wave–wave and wave–body interactions. For completeness, we outline the main steps. We express the nonlinear free-surface boundary conditions in the form of Zakharov (1968):

$$\left.\begin{aligned} \eta_t + \nabla_x\eta\cdot\nabla_x\Phi^S - (1+\nabla_x\eta\cdot\nabla_x\eta)\Phi_z(\boldsymbol{x},\eta,t) = 0, \\ \Phi^S_t + g\eta + \tfrac{1}{2}\nabla_x\Phi^S\cdot\nabla_x\Phi^S - \tfrac{1}{2}(1+\nabla_x\eta\cdot\nabla_x\eta)\Phi_z^2(\boldsymbol{x},\eta,t) = 0, \end{aligned}\right\} \tag{5.1}$$

where $\Phi^S(\boldsymbol{x},t) = \Phi(\boldsymbol{x},\eta(\boldsymbol{x},t),t)$ is the surface potential evaluated at the surface elevation $\eta(\boldsymbol{x},t)$. Given the initial conditions $\eta(\boldsymbol{x},0)$ and $\Phi^S(\boldsymbol{x},z,0)$, (5.1) are the evolution equations which integrate the initial-value problem provided that the surface vertical velocity $\Phi_z(\boldsymbol{x},\eta,t)$ is obtained from the boundary-value problem at each time.

To solve the boundary-value problem, we consider regular perturbation expansions in both the bottom undulation $\zeta(\boldsymbol{x})$ and the instantaneous free surface $\eta(\boldsymbol{x},t)$. In principle, the free-surface and bottom steepnesses (ϵ_f, ϵ_b) can be treated separately and different perturbation orders (M_f, M_b) considered in the HOS method. For simplicity, we assume $\epsilon_f \sim \epsilon_b = O(\epsilon)$ and consider expansions up to the same (arbitrary) order $M_f = M_b = M$ in the free-surface/bottom wave slope ϵ. (Because of the efficiency of the HOS method, keeping more terms than necessary for either ϵ_f or ϵ_b does not create a substantial computational burden in practice but simplifies the description in what follows and also somewhat the programming.) For the potential, we have

$$\Phi(\boldsymbol{x},z,t) = \sum_{m=1}^{M}\Phi^{(m)}(\boldsymbol{x},z,t), \tag{5.2}$$

where $\Phi^{(m)} = O(\epsilon^m)$ are the perturbation potentials.

We then expand the surface potential Φ^S and the bottom boundary condition (2.1) in separate Taylor series with respect to the mean surfaces $z = 0$ and $z = -h$ respectively. After collecting terms at the respective orders, we obtain for successive orders a sequence of Dirichlet conditions on $z = 0$:

$$\left.\begin{aligned} &\Phi^{(1)}(\boldsymbol{x},0,t) = \Phi^S, \\ &\Phi^{(m)}(\boldsymbol{x},0,t) = -\sum_{\ell=1}^{m-1}\frac{\eta^\ell}{\ell!}\frac{\partial^\ell}{\partial z^\ell}\Phi^{(m-\ell)}\bigg|_{z=0}, \quad m = 2,3,\cdots,M; \end{aligned}\right\} \tag{5.3}$$

and Neumann conditions on $z = -h$:

$$\left.\begin{aligned} \Phi_z^{(1)}(\boldsymbol{x}, -h, t) &= 0, \\ \Phi_z^{(m)}(\boldsymbol{x}, -h, t) &= \sum_{\ell=1}^{m-1} \left\{ \frac{\partial}{\partial x} \left[\frac{\zeta^\ell}{\ell!} \frac{\partial^{(\ell-1)}}{\partial z^{(\ell-1)}} \Phi_x^{(m-\ell)} \Big|_{z=-h} \right] \right. \\ &\quad \left. + \frac{\partial}{\partial y} \left[\frac{\zeta^\ell}{\ell!} \frac{\partial^{(\ell-1)}}{\partial z^{(\ell-1)}} \Phi_y^{(m-\ell)} \Big|_{z=-h} \right] \right\}, \quad m = 2, 3, \ldots, M. \end{aligned}\right\} \tag{5.4}$$

At each order m, the perturbation potential $\Phi^{(m)}$ satisfies the Laplace equation in the mean fluid domain $-h < z < 0$, (5.3) on $z = 0$, and (5.4) on $z = -h$. For computations, the problem is typically closed by assuming periodic conditions in the horizontal plane, say, $[-L_x, L_x] \times [-L_y, L_y]$.

In a spectral approach, we represent $\Phi^{(m)}$ in terms of global basis functions which satisfy the field equation and homogeneous surface and bottom conditions. Thus, we write, $\Phi^{(m)} = \alpha^{(m)} + \beta^{(m)}$, where

$$\alpha^{(m)}(\boldsymbol{x}, z, t) = \sum_{n=-N/2}^{N/2} \alpha_n^{(m)}(t) \frac{\cosh[|\boldsymbol{K}_n|(z+h)]}{\cosh(|\boldsymbol{K}_n|h)} \mathrm{e}^{\mathrm{i}\boldsymbol{K}_n \cdot \boldsymbol{x}} + \text{c.c.}, \tag{5.5}$$

$$\beta^{(m)}(\boldsymbol{x}, z, t) = \beta_0^{(m)} z + \sum_{n=-N/2}^{N/2} \beta_n^{(m)}(t) \frac{\sinh(|\boldsymbol{K}_n|z)}{|\boldsymbol{K}_n| \cosh(|\boldsymbol{K}_n|h)} \mathrm{e}^{\mathrm{i}\boldsymbol{K}_n \cdot \boldsymbol{x}} + \text{c.c.} \tag{5.6}$$

Here, $\boldsymbol{K}_n = (K_{xn}, K_{yn}) = (n\pi/L_x, n\pi/L_y)$ is the wavenumber vector of the Fourier series. Note that $\alpha^{(m)}$ and $\beta^{(m)}$ respectively satisfy the zero Neumann condition on $z = -h$ and the zero Dirichlet condition on $z = 0$. (In general, the number of free-surface and bottom wavenumbers, say N_f and N_b, can be chosen independently in the HOS method. For simplicity, we use $N_f = N_b = N$).

The perturbation modal amplitudes, $\alpha_n^{(m)}$ and $\beta_n^{(m)}$, are determined by taking the inner product of $\mathrm{e}^{\mathrm{i}\boldsymbol{K}_n \cdot \boldsymbol{x}}$ with (5.3) and (5.4) respectively. For smooth (periodic) $\Phi^{(m)}$, $\alpha_n^{(m)}$ and $\beta_n^{(m)}$ decay exponentially with increasing wavenumber $|\boldsymbol{K}_n|$. After the boundary-value problem for $\Phi^{(m)}$ is solved successively up to the desired order M, the vertical velocity on the free surface is determined from

$$\Phi_z(\boldsymbol{x}, \eta, t) = \sum_{m=1}^{M} \sum_{\ell=0}^{M-m} \frac{\eta^\ell}{\ell!} \frac{\partial^{\ell+1}}{\partial z^{\ell+1}} \Phi^{(m)}(\boldsymbol{x}, 0, t). \tag{5.7}$$

The evolution equations (5.1) are then integrated in time for the new values of Φ^S and η. The complete solution of the nonlinear initial boundary-value problem is obtained by repeating this process starting from initial conditions.

5.2. *Implementation*

The implementation of the HOS method for a solution up to a given order M consists of two main parts:

(*a*) Given the surface elevation $\eta(\boldsymbol{x}, t)$ and potential $\Phi^S(\boldsymbol{x}, t)$ at time instant t, the modal amplitudes $\alpha_n^{(m)}$ and $\beta_n^{(m)}$ subject to the Dirichlet condition (5.3) and the Neumann condition (5.4) are solved using a pseudo-spectral method. Specifically, all spatial derivatives of $\Phi^{(m)}$, Φ^S and η are evaluated in wavenumber space while nonlinear products are calculated in physical space at a discrete set of points $\boldsymbol{x}_j$. For periodic boundary conditions using the Fourier expansions (5.5) and (5.6), $\boldsymbol{x}_j$

N_w	$M=2$	$M=3$	$M=4$
16	0.7250	0.7080	0.7080
24	0.7115	0.7111	0.7113
32	0.7115	0.7112	0.7113

TABLE 1. Convergence of the class I Bragg reflection coefficient, $R=a_r/A$, with increasing number of wavelengths $N_w = 2L/\lambda$ of the computational domain and for different orders M. The fixed parameters are: $L_0/\lambda_b = 10$, $k_b d = 0.31$, $d/h = 0.16$, $k_b/k = 2$, $kA = 0.05$; and $N/N_w = 64$, $T/\Delta t = 64$, $T_s/T = 20$.

are equally spaced and fast-Fourier transforms are used to project between the wavenumber and physical domains. At each order, (5.3) and (5.4) are solved in wavenumber space by equating Fourier modes, and the number of operations required is $O(N \ln N)$. For perturbations up to order M, the operation count is then $O(MN \ln N)$ per time step.†

(*b*) The evolution equations (5.1) are integrated in time to obtain the new values $\eta(\boldsymbol{x}, t + \Delta t)$ and $\Phi^S(\boldsymbol{x}, t + \Delta t)$. For the present computations, we use a fourth-order Runge–Kutta integrator with constant time step Δt.

The two steps (*a*)–(*b*) are repeated starting from initial values.

5.3. *Convergence tests*

To demonstrate the accuracy and convergence of the HOS method, we use as an illustration a class I Bragg reflection problem of an incident surface wave, wavenumber $k = 2\pi/\lambda$, propagating normally over a patch of uniformly sinusoidal bottom ripples, wavenumber $k_b = 2\pi/\lambda_b$.

For this example, the following parameters are used: the length of the bottom patch $L_0/\lambda_b = 10$; the slope of the bottom undulations $k_b d = 0.31$; and mean depth $d/h = 0.16$. For the incident wave, we use an exact finite-depth Stokes wave (Schwartz 1974), wavenumber $k = 2\pi/\lambda = k_b/2$; period T; and wave slope $\epsilon \equiv kA = 0.05$, where $2A \equiv \eta_{max} - \eta_{min}$. To demonstrate numerical convergence, we vary the order M, the numbers of free-surface/bottom modes N, the length of the (periodic) computational domain $2L = N_w\lambda$, the time step for the fourth-order Runge–Kutta integration Δt, and the total simulation time T_s.

Similar to the wave–body interaction problem of Liu *et al.* (1992), the radiation condition at the far field is replaced by periodic boundary conditions in the horizontal direction. The bottom ripple patch is placed at the centre of the computational domain, $[-L_0/2, L_0/2]$, and errors associated with the periodic boundaries are controlled by successively increasing the length, $2L = N_w\lambda$, of the computational domain. Table 1 shows the results for the class I Bragg reflection coefficient $R \equiv a_r/A$, where a_r is the amplitude of the Bragg reflected wave. The convergence with the length of the computational domain, $2L = N_w\lambda$, and with the order M is evident. For $N_w = 32$, for example, the reflection coefficient R has converged to four significant figures.

For moderate bottom and free-surface slopes (cf. Dommermuth & Yue 1987) and orthogonal global basis functions, the convergence of (5.5) and (5.6) with respect to N is expected to be exponentially rapid. Table 2 shows the convergence of the class I Bragg reflection coefficient with increasing N/N_w (number of Fourier modes per

† At first glance, the effort for computing the summation in (5.7) appears to be proportional to M^2. After the summation is rewritten as $\sum_{\ell=0}^{M}(\eta^\ell/\ell!)(\partial^{\ell+1}/\partial z^{\ell+1})\sum_{m=1}^{M-\ell}\Phi^{(m)}$, however, it becomes clear that the effort in fact is linearly proportional to M.

N/N_w	$M=2$	$M=3$	$M=4$
16	0.7125	0.7110	0.7155
32	0.7110	0.7106	0.7107
64	0.7115	0.7112	0.7113

TABLE 2. Convergence of the class I Bragg reflection coefficient, $R=a_r/A$, with increasing number of spectral modes N for different orders M. The fixed parameters are: $L_0/\lambda_b = 10$, $k_b d = 0.31$, $d/h = 0.16$, $k_b/k = 2$, $kA = 0.05$; and $N_w=2L/\lambda = 32$, $T/\Delta t = 64$, $T_s/T = 20$.

T_s/T	$M=2$	$M=3$	$M=4$
11	0.7615	0.7550	0.7510
12	0.7455	0.7352	0.7320
13	0.7310	0.7265	0.7250
14	0.7200	0.7180	0.7170
15	0.7150	0.7130	0.7125
16	0.7116	0.7113	0.7112
17	0.7115	0.7114	0.7111
18	0.7113	0.7112	0.7112
19	0.7114	0.7113	0.7112
20	0.7115	0.7112	0.7113

TABLE 3. Convergence of the class I Bragg reflection coefficient, $R = a_r/A$, with increasing total simulation time T_s/T for different orders M. The fixed parameters are: $L_0/\lambda_b = 10$, $k_b d = 0.31$, $d/h = 0.16$, $k_b/k = 2$, $kA = 0.05$; and $N_w=2L/\lambda = 32$, $T/\Delta t = 64$, $N/N_w = 64$.

surface wavelength) for different orders M. The results in table 2 confirm the expected exponential convergence of the solution.

For a finite bottom patch, our typical interest is in the steady-state values of the resonant wave amplitudes. To obtain reliable results in an initial-value approach, we increase the simulation time T_s successively until the predicted values reach steady state. Table 3 shows the convergence of R with the simulation time T_s/T for different orders M. Steady-state values for R are reached rapidly (to almost four decimals) after $T_s/T \sim 15$ (for $L_0/\lambda_b = 10$).

The convergence with the time step $\Delta t/T$ of the present fourth-order Runge–Kutta integration scheme is also tested systematically, recovering the expected $O(\Delta t/T)^4$ global error. These are not presented separately (similar convergence results can be found in Liu *et al.* 1992). Unless otherwise stated, for all subsequent computations in this paper, we use $N_w = 32$ and $N = 64N_w$ per horizontal dimension, $T_s/T = 15$–25, and $T/\Delta t = 64$. Based on the foregoing numerical tests, we anticipate the maximum error in the predicted wave amplitudes to be less than 1%.

We remark in closing this section that because of the high efficiency of the HOS method, computational costs are relatively small for all the cases we present. For the tests above with $M = 4$ and $N = 2048$, for example, the HOS simulation requires only $O(10^{-2})$ CPU s per time step (less than 1 CPU s per wave period) on a (single processor) Cray-YMP computer. The computational parameters we have chosen are therefore unnecessarily conservative, and have we not resorted to many of the techniques (e.g. taper filtering of the far-field waves) which we have found useful for larger-scale practical applications (Liu 1994).

6. Numerical results

In this section, we apply the HOS method of §5 to simulate nonlinear wave interactions with an underlying patch of bottom ripples. Both two- and three-dimensional high-order computations are performed. The primary focus is on the three classes of Bragg resonances analysed in §§3, 4. We present results for known Bragg resonance cases for which we make comparisons to available experimental data and theoretical (regular and multiple-scale perturbation) solutions. We also present illustrative examples of the new class II (bi-directional bottom ripples) and class III Bragg resonance interactions. In all cases, we choose physical parameters which correspond exactly to experimental values or which accentuate the solution features of the resonance in question.

6.1. *Class I Bragg resonance*

We consider the development of incident and Bragg reflected waves, wavenumbers $\boldsymbol{k}_1$ and $\boldsymbol{k}_2$ respectively, over a bottom patch with a single sinusoidal ripple of wavenumber $\boldsymbol{k}_b$. If the class I Bragg condition (3.4) is satisfied, the reflected wave associated with $\boldsymbol{k}_2$ is amplified as a result of resonant quadratic interaction between the incident wave and the bottom variation. This condition has been studied experimentally by Davies & Heathershaw (1984). For small incident wave and bottom slopes, reflection at or near the class I Bragg resonance is predicted well by multiple-scales perturbation theory under the assumption of linearized surface waves (Mei 1985). Here we obtain direct computational demonstration of class I Bragg resonance using the HOS method which also allows us to investigate higher-order nonlinear effects of the free surface and bottom on this class of resonant reflection.

To compare with experiments, we choose a case of Davies & Heathershaw (1984) with $L_0/\lambda_b = 10$ (a bottom patch containing 10 complete sinusoidal ripples) and bottom slope $k_b d = 0.31$. In addition to the normal incidence they consider, we also study the more general case of oblique incidence. We perform direct nonlinear ($M = 3$) simulations to obtain the steady-state (limit-cycle) free-surface elevation $\eta(\boldsymbol{x}, t)$ from which the reflection and transmission wave amplitudes are extracted (see the Appendix).

6.1.1. *Normal incidence*

In this case, $\boldsymbol{k}_1$ and $\boldsymbol{k}_b$, and consequently, $\boldsymbol{k}_2$, are in the same direction and the problem is two-dimensional. Figure 5 shows the HOS solution, $M = 3$ (the results for $M = 2$ and 3 hardly differ for this case, cf. §5.3) for the spatial variation of the Bragg reflection coefficient $R(x)$ at the (linearized) Bragg resonance value, $k \equiv k_1 = k_2 = k_b/2$, for two different mean water depths corresponding to $d/h = 0.1$ and 0.14. (The small oscillations in the HOS results are due to the use of Gota & Suzuki (1976)'s simple formula to extract the steady-state coefficient from time history.) For comparison, we also show results from the experiments of Davies & Heathershaw (1984), and the multiple-scale perturbation theory of Mei (1985). The agreement is satisfactory, with all three results showing the expected (cf. (4.8)) linear variations and slopes of $R(x)$ over the bottom patch ($x/\lambda_b \in [-5, 5]$).

A more interesting comparison is to vary k/k_b and observe the variation of the Bragg reflection coefficient in the neighborhood of the class I Bragg resonance. This is shown in figure 6 for the case $d/h = 0.16$. The HOS results (with $M = 3$) are compared with the measured values of Davies & Heathershaw (1984) and the perturbation solution of Mei (1985). The agreement among them is overall satisfactory. One effect seen in the experimental data is the downshift in wavenumber of the peak Bragg reflected

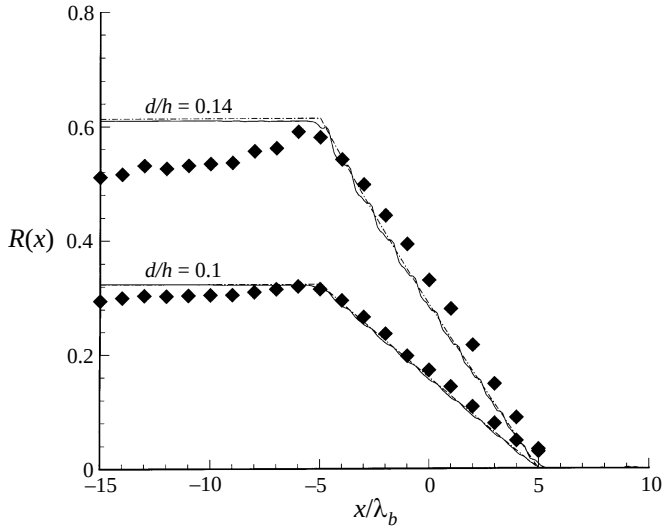

FIGURE 5. Spatial variation of the class I Bragg reflection coefficient over a bottom ripple patch $-5\lambda_b < x < 5\lambda_b$, for $kA = 0.05$, $k_b d = 0.31$. Results plotted are: experiments (Davies & Heathershaw 1984) (◆); perturbation theory (Mei 1985) (— · —); and HOS computations for $M = 3$ (——).

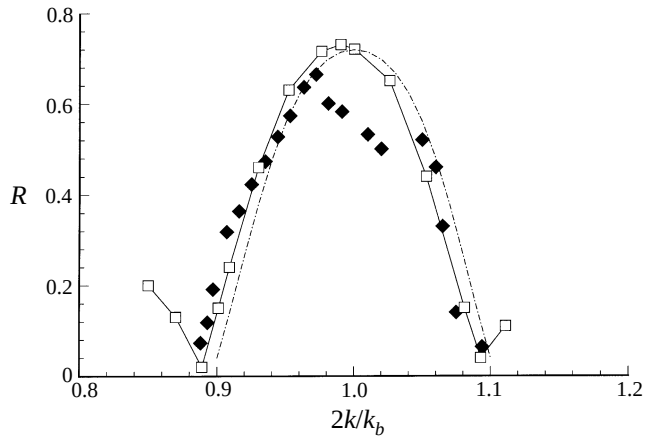

FIGURE 6. Class I Bragg reflection coefficient near the linearized class I condition, $2k/k_b = 1$, for $kA = 0.05$, $k_b d = 0.31$, $d/h = 0.16$. Results plotted are: experiments (Davies & Heathershaw 1984) (◆); perturbation theory (Mei 1985) (— · —); and HOS computations for $M = 3$ (□).

wave relative to the linearized Bragg point, $2k/k_b = 1$. This is predicted by the present high-order computation but is not present in Mei's perturbation theory.

The resonant wavenumber downshift can in general be attributed to nonlinear effects associated with the problem. In the present case, free-surface nonlinearity is manifest primarily in the Stokesian decrease in surface wavenumber with increasing steepness which should result in an increase of the resonant (linearized) value of k relative to k_b. On the other hand, nonlinear effects associated with the bottom variations would in general lead to a downshift of the resonant wavenumber. To obtain an estimate of this effect, we assume small-amplitude surface waves and slowly

varying bottom variations, and write the dispersion relation as

$$\omega^2 = gk \tanh k[h + \zeta(x)]. \tag{6.1}$$

For $k\zeta \ll kh = O(1)$, we expand the wavenumber $k(x)$ in a perturbation series:

$$k(x) = k_0 + k_1(x) + k_2(x) + \cdots, \tag{6.2}$$

where k_0 is independent of x and given by $\omega^2 = gk_0 \tanh k_0 h$. Substituting (6.2) into (6.1) and solving for the perturbation wavenumbers, we obtain

$$\frac{k_1(x)}{k_0} = -\frac{2k_0\zeta}{2k_0h + \sinh 2k_0h}, \tag{6.3}$$

and

$$\frac{k_2(x)}{k_0} = \frac{2(k_0\zeta)^2}{(2k_0h + \sinh 2k_0h)^3}\,[4k_0h + (3 + \cosh 2k_0h)\sinh 2k_0h]\,. \tag{6.4}$$

After taking the spatial average $\overline{(\ )}$ of $k(x)$, it follows that

$$\bar{k} = k_0 + \frac{(k_0|\zeta|)^2}{(2k_0h + \sinh 2k_0h)^3}\,[4k_0h + (3 + \cosh 2k_0h)\sinh 2k_0h] + \cdots. \tag{6.5}$$

The second term in (6.5) is always positive, so that bottom nonlinearity in general increases the average free-surface wavenumber and thus shifts the peak Bragg reflection to a lower wavenumber relative to the linearized Bragg point. Note that non-constant $k(x)$ also leads to evanescent wave modes which have been suggested as a cause of the resonant frequency downshift (Guazzelli *et al.* 1992).

Nonlinear free-surface and bottom effects on class I Bragg reflection are obtained more systematically by repeating the simulations varying the free-surface and bottom wave steepnesses. The results are reported in Liu (1994) and are not repeated here. Our results indicate that nonlinearities of the free-surface and bottom boundaries are second order in the associated steepness and are generally small as far as the Bragg reflected wave amplitude is concerned.

6.1.2. *Oblique incidence*

As indicated by (3.4), class I Bragg resonance also occurs when the incident wave ($\boldsymbol{k}_1$) is oblique to the bottom ripples ($\boldsymbol{k}_b$). We consider the same bottom geometry as in §6.1.1 ($d/h = 0.16$) but vary the angle θ between $\boldsymbol{k}_b$ and $\boldsymbol{k}_1$ (measured counter-clockwise from $\boldsymbol{k}_b$ which we set parallel to the x-axis). The problem is now three-dimensional, and for the numerical simulation, we employ a (doubly periodic) computational domain of dimensions $N_{wx}\lambda_x$ by $N_{wy}\lambda_y$, where the incident wavelength is $\lambda = 2\pi/|\boldsymbol{k}_1| = \lambda_x \cos\theta = \lambda_y \sin\theta$ and $(N_{wy}/N_{wx})^{1/2} = \tan\theta$. The simulations are carried out until steady-state free-surface elevation is obtained, and the reflection and transmission coefficients are determined from (A 4) and (A 5).

Figure 7 plots the class I Bragg reflection coefficient at linearized Bragg resonance (3.4) as a function of the oblique incidence angle θ. Comparison is made to the perturbation theory of Mei, Hara & Naciri (1988), and the agreement is excellent. For both the numerical solution and the perturbation theory, figure 7 shows that at the critical incidence angle of $\theta = \pi/4$, wave propagation is unaffected by the presence of the bottom ripples. For oblique incidence, the magnitude of the incident wavenumber kh increases (in order to still satisfy Bragg condition) and the relative effect of the bottom variations diminshes. Thus the downshift observed in figure 6 as well as the Bragg resonance effect itself become weak as θ increases.

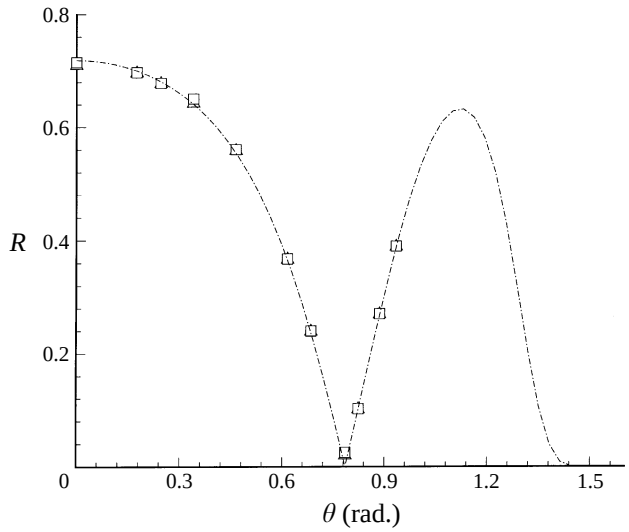

FIGURE 7. Class I Bragg reflection coefficient as a function of incidence wave angle θ relative to the bottom ripples, for $kA = 0.05$, $k_b d = 0.31$, $d/h = 0.16$. Results plotted are: perturbation theory (Mei *et al.* 1988) (— · —); and HOS computations for $M = 2$ (△), and $M = 3$ (□).

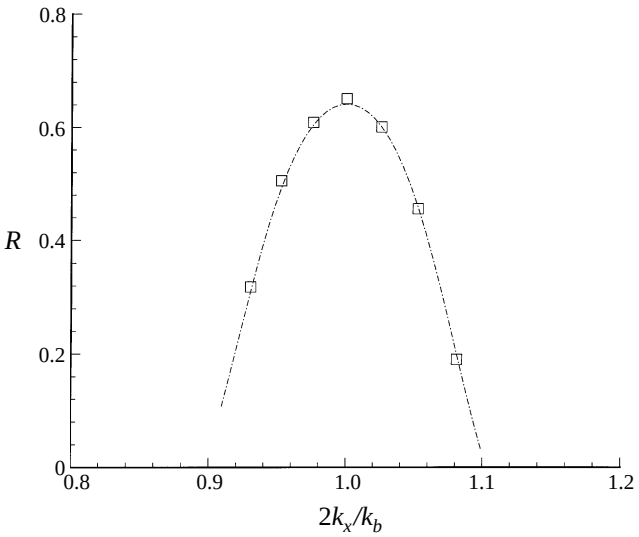

FIGURE 8. Class I Bragg reflection coefficient near the linearized class I condition, $2k_x = 2k\cos\theta = k_b$, for a fixed (oblique) incidence $\theta = 19.47°$, and $kA = 0.05$, $k_b d = 0.31$, $d/h = 0.16$. Results plotted are: perturbation theory (Mei *et al.* 1988) (— · —); and HOS computations for $M = 3$ (□).

At a fixed incidence angle of $\theta = 19.47° = \tan^{-1}(1/8)^{1/2}$, figure 8 shows the computed Bragg reflection coefficient in the neighbourhood of the class I resonance point compared to the perturbation theory of Mei *et al.* (1988). The comparison is excellent.

6.2. *Class II Bragg resonance*

When the bottom consists of doubly sinusoidal ripples, say wavenumbers $\boldsymbol{k}_{b1}$ and $\boldsymbol{k}_{b2}$, class II Bragg resonance occurs when (3.5) is satisfied. Although class II Bragg

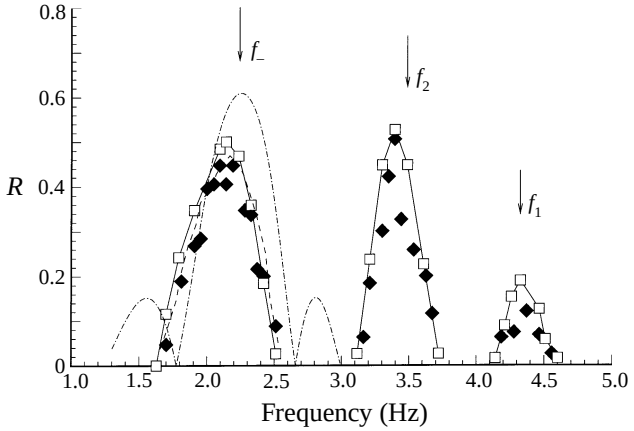

FIGURE 9. Bragg reflection coefficient for a wave incident normally upon a doubly periodic ripple bottom in the neighbourhood of frequencies satisfying class I Bragg resonances: f_1 at $k = k_{b1}/2$; f_2 at $k = k_{b2}/2$; and sub-harmonic class II Bragg resonance: f_- at $k = (k_{b1} - k_{b2})/2$. Results plotted are: experiments (Guazzelli *et al.* 1992) (◆), HOS computations for M=3 (□); and, near f_-, SAMM numerical results (Guazzelli *et al.* 1992) (- - -), and perturbation theory (Rey *et al.* 1996) (— · —).

resonance involves quartet interactions (two bottom components) and is in theory one order higher than class I Bragg reflection, for realistic bottom conditions the resonant wave can in fact have amplitudes which are comparable in magnitude to class I reflection (and occurs at distinct frequencies). This has been observed, for example, in the experiments of Guazzelli *et al.* (1992) who consider the two-dimensional problem of normal incidence of a wave over a bottom containing doubly sinusoidal ripples.

6.2.1. *Unidirectional bottom undulations*

We first study the case of Guazzelli *et al.* (1992) involving normal incidence over bottom undulations containing unidirectional doubly sinusoidal (two different wavelengths) ripples. The bottom topography they consider is: ripple patch length $L_0 = 48$ cm, ripple amplitudes $d_1 = d_2 = 1$ cm, and ripple wavenumbers $k_{b1} = \pi/3$ cm^{-1} and $k_{b2} = \pi/2$ cm^{-1}, and mean water depth $h = 4$ cm. For these conditions, we perform HOS ($M = 3$) simulations for a range of incident wavenumber k. The transmission and reflection coefficients are obtained from (A 4) and (A 5) after steady-state wave elevation is reached.

Figure 9 shows the Bragg reflection coefficient in the neighbourhood of the two class I and the sub-harmonic class II Bragg resonances. The HOS results are compared with the experimental and SAMM numerical values of Guazzelli *et al.* (1992) and the multiple-scale perturbation solution of Rey *et al.* (1996). The HOS computations agree well with measurements at all three resonances for both the peak frequencies and amplitudes. As in the case of class I Bragg resonance (see figure 6), perturbation theory does not predict the downshift of the peak frequency, and in this case also overestimates the peak reflection amplitude for the class II Bragg resonance. As pointed out by Guazzelli *et al.* (1992), the downshift at f_- is predicted by SAMM which accounts for bottom nonlinearities. Note that, for the conditions chosen, the sub-harmonic class II reflected wave is comparable in magnitude to the lower-order class I Bragg reflection and is appreciable relative to the incident wave.

Finally, we note that, in theory, a super-harmonic class II Bragg resonance also exists in this case and is observed in HOS simulations. In this case, the amplitude of

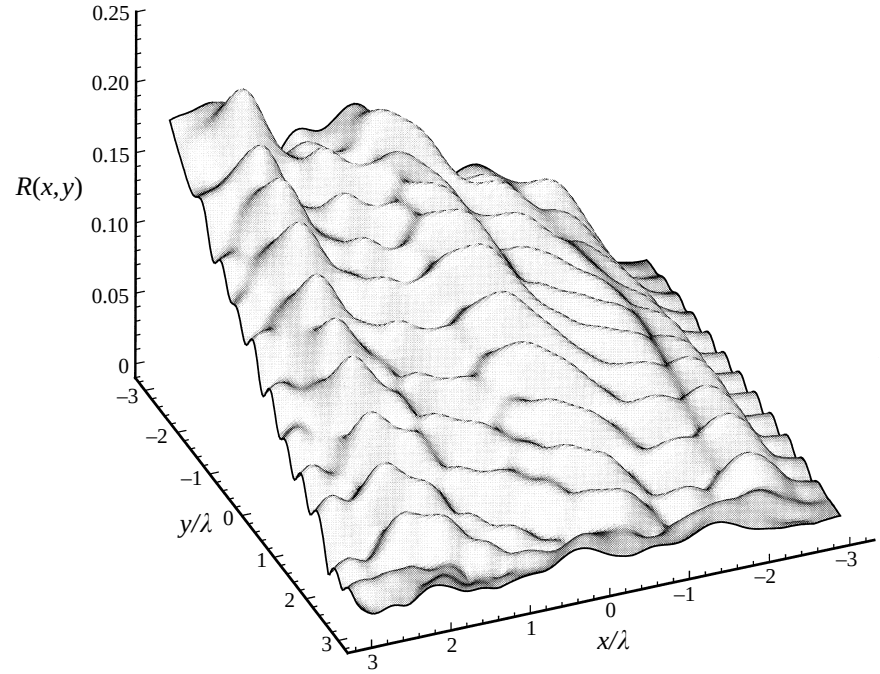

FIGURE 10. Spatial variation of class II Bragg reflection coefficient for a wave incident upon a bottom patch ($|x, y| < 3\lambda$) of doubly periodic ripples, $\boldsymbol{k}_{b1} = (k/2, k)$, $\boldsymbol{k}_{b2} = (k/2, 0)$, and $\boldsymbol{k}_1 = (k, 0)$, $\boldsymbol{k}_r = (0, -k)$, $kd_1 = kd_2$=0.15, $kA = 0.05$. Results are from HOS simulation with $M = 3$.

this high-wavenumber super-harmonic class II reflected wave is, however, negligibly small relative to those associated with class I and sub-harmonic class II resonances shown in figure 9.

6.2.2. *Bidirectional bottom undulations*

A case of class II Bragg resonance not considered by Guazzelli *et al.* (1992) but which should be of practical interest is the three-dimensional problem of a wave incident upon a bottom patch composed of bidirectional sinusoidal ripples. To be specific, and to illustrate super-harmonic class II Bragg reflection, we choose a case with bottom wavenumbers $\boldsymbol{k}_{b1} = (k/2, k)$ and $\boldsymbol{k}_{b2} = (k/2, 0)$, and an incident wave parallel to one of them with wavenumber $\boldsymbol{k}_1 = (k, 0)$. It follows from the class II condition (3.5) that a super-harmonic Bragg reflected wave will be resonantly excited which has wavenumber, $\boldsymbol{k}_r = (0, -k)$, perpendicular to the incident wave.

We verify this with direct HOS simulation. For definiteness, we choose incident wave steepness $kA = 0.05$, bottom slopes $kd_1 = kd_2 = 0.1$, mean water depth $kh = 1.5$, and a bottom-ripple patch of dimensions $kL_{0x} = kL_{0y} = 12\pi$ centred at the origin. Figure 10 shows the steady-state spatial variation over the bottom patch of the amplitude of the super-harmonic class II reflected wave, wavenumber $\boldsymbol{k}_r = (0, -k)$. The maximum Bragg reflection coefficient in this case is about 0.2. Additional HOS simulations confirm that the maximum amplitude of this class II Bragg reflected wave depends quadratically on the bottom slope and linearly on the length of the bottom patch (in the direction of $\boldsymbol{k}_r$).

6.3. *Class III Bragg resonance*

We now consider the third-order class III Bragg resonance which occurs when free-surface nonlinearity is included. The resonance condition to be satisfied is (3.7) which shows that the resonance is a result of interactions among one bottom and three surface wave components. Unlike class I and class II Bragg reflections, the class III resonant wave may be reflected or transmitted (relative to the incident waves) depending on the wave–bottom geometry (cf. figures 2*a* and 2*b*). Although this class of resonance can be anticipated directly from theoretical wave–wave interaction considerations, and may have implications (comparable to class I and II Bragg reflections and nonlinear surface wave–wave interactions) for coastal wave propagation, it appears not to have been investigated so far.

To illustrate the mechanism of this class of Bragg resonance, we consider the simplest possible case involving a single incident wave, wavenumber $\boldsymbol{k}$, frequency ω, incident normally or obliquely upon uniformly sinusoidal ripples of a single wavenumber $\boldsymbol{k}_b$. For this case, the class III Bragg resonance condition (3.7) can be satisfied by accounting for the incident wave twice (i.e. $\boldsymbol{k}_2 = \boldsymbol{k}_1 \equiv \boldsymbol{k}$), and a reflected sub-harmonic ($\boldsymbol{k}_3 \equiv \boldsymbol{k}_r = 2\boldsymbol{k} - \boldsymbol{k}_b$) or transmitted super-harmonic ($\boldsymbol{k}_3 \equiv \boldsymbol{k}_t = 2\boldsymbol{k} + \boldsymbol{k}_b$) wave is generated at double-frequency (2ω) as a result of quartet interactions among the surface waves and the bottom ripple. In the following, both HOS simulation results and regular perturbation solutions (§4) are presented to elucidate basic characteristics of the generated sub- and super-harmonic double-frequency waves associated with the class III Bragg resonance.

6.3.1. *Normal incidence*

For normal incidence, all wavenumbers are in the same direction and the problem is two-dimensional. For numerical illustration, we choose a patch of bottom ripples with the patch width $L_0 = 36\lambda_b$ and the bottom steepness $k_b d = 0.25$ in a mean depth of $k_b h = 2.642$. For such a bottom topography, according to (3.9), class III Bragg resonance occurs when the incident wavenumber is $k \approx 0.227 k_b$ resulting in the generation of a sub-harmonic wave, wavenumber $k_r \approx 0.546 k_b$, which is reflected (i.e. propagates in a direction opposite to the incident wave).

Figure 11 shows the variation of the sub-harmonic reflection coefficient in the neighbourhood of the class III resonance wavenumber ($k = 0.227 k_b$). The numerical results are obtained from HOS using orders $M = 3$ and $M = 4$. For both incident wave steepnesses $kA = 0.03$ and 0.06, it is clear that the class III Bragg phenomenon is captured well by accounting for interactions up to third order, $M = 3$.

For the relatively small surface and bottom steepnesses, the regular perturbation solution of §4 provides a useful comparison. On the basis of the analysis of §4, the perturbation solution for the reflected double-frequency wave amplitude is obtained to be

$$A_r(k_r) = \left[g\mathscr{B}_2^{(3)} - \mathscr{F}^{(3)} \cosh k_r h \right] \frac{k_r L_0 \sinh k_r h \sin[(k_r + 2k - k_b)L_0/2]}{\omega g(2k_r h + \sinh 2k_r h)[(k_r + 2k - k_b)L_0/2]} \tag{6.6}$$

where the coefficients $\mathscr{B}_2^{(3)}$ and $\mathscr{F}^{(3)}$ are given by (4.18) and (4.19), respectively. This is also plotted in figure 11. For both incident wave steepnesses $kA = 0.03$ and 0.06, it is seen that the comparisons are excellent except that the location of peak reflection is downshifted in wavenumber relative to the linearized Bragg point. Unlike the earlier class I and II resonances, nonlinear surface wave interactions enter the picture, and the downshift is greater for larger surface wave steepness in this case.

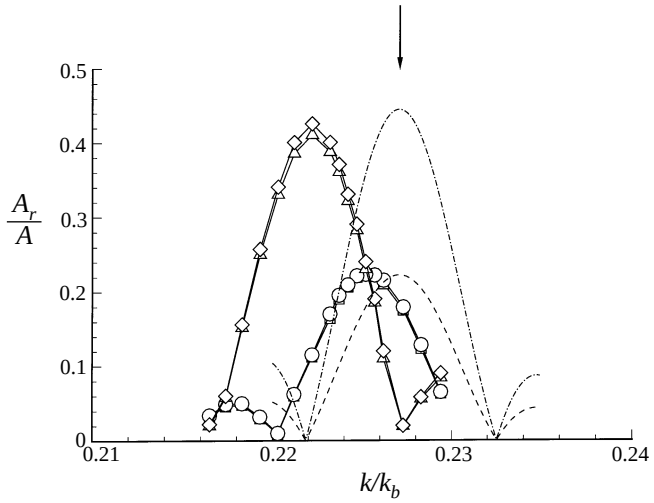

FIGURE 11. Class III sub-harmonic Bragg reflection coefficient near the linearized Bragg resonance condition, $k/k_b = 0.227$ (indicated by $\downarrow$) for $k_b h = 2.642$, $k_b d = 0.25$ and $L_0 = 36\lambda_b$. Results for two incident steepnesses are given: (i) $kA = 0.03$ for HOS simulations with $M = 3$ (—□—), $M = 4$ (—○—); and regular perturbation theory (- - -); and (ii) $kA = 0.06$ for HOS simulations with $M = 3$ (—△—), $M = 4$ (—◇—), and regular perturbation theory (— · —).

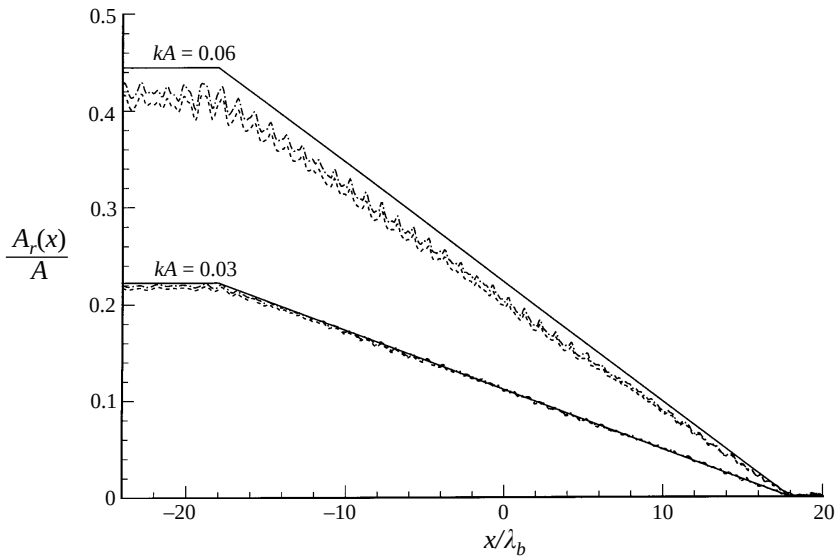

FIGURE 12. Spatial variation of the class III sub-harmonic Bragg reflected wave amplitude over a bottom patch ($|x|/\lambda_b \leqslant 18$) of sinusoidal ripples, $k_b d = 0.25$ and $k_b h = 2.642$. The perturbation solution (——) is obtained at the exact linearized class III condition, $k/k_b = 0.227$; while the HOS simulations with $M = 3$ (- - -) and $M = 4$ (— · —) are obtained at $k/k_b = 0.225$ for $kA = 0.03$ and $k/k_b = 0.222$ for $kA = 0.06$, corresponding respectively to peak amplitudes in the reflected wave (see figure 11).

Figure 12 shows the comparison between the simulation results and the regular perturbation solution for the spatial variation of the sub-harmonic class III Bragg reflection coefficient over the bottom ripple patch. For the present bottom geometry,

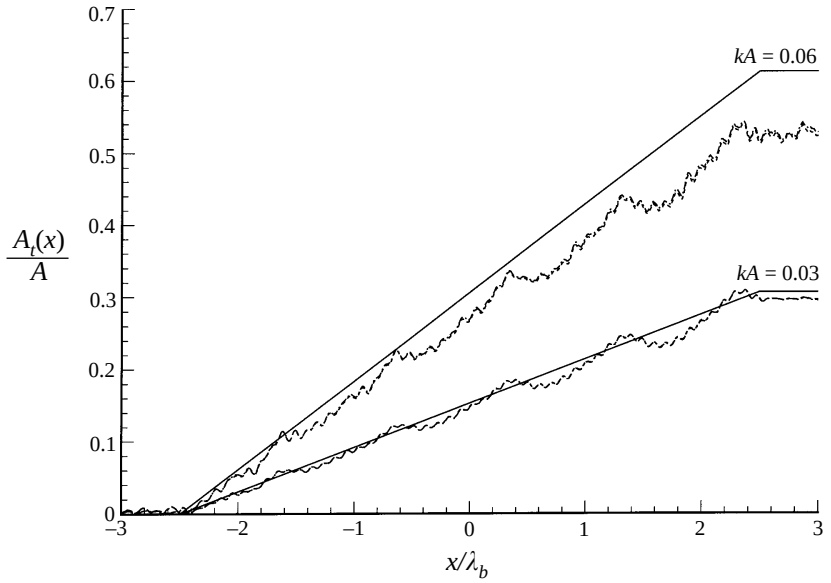

FIGURE 13. Spatial variation of the class III super-harmonic Bragg transmitted wave amplitude over a bottom patch ($|x|/\lambda_b \leqslant 2.5$) of sinusoidal ripples, $k_b d = 0.025$ and $k_b h = 0.325$. The perturbation solution (——) is obtained at the exact linearized class III condition, k/k_b=2.031; while the HOS simulations with $M = 3$ (- - -) and $M = 4$ (— · —) are obtained at $k/k_b = 2.021$ for $kA = 0.03$ and $k/k_b = 2.025$ for $kA = 0.06$, corresponding respectively to peak amplitudes in the transmitted wave.

the perturbation solution of the reflected sub-harmonic wave amplitude (A_r) over the bottom ripple is obtained from (4.23) to be

$$A_r(x) \approx 0.0058(kA)^2(k_b d)(L_0/2 - x), \quad -L_0/2 < x < L_0/2. \tag{6.7}$$

The comparison is excellent for the smaller incident wave steepness case of $kA = 0.03$, and, as expected, is less so but still satisfactory for the larger steepness case of kA=0.06, where the perturbation theory somewhat overestimates A_r.

For class III super-harmonic wave transmission, analogous results can be obtained. For illustration, we consider a case where $L_0 = 5\lambda_b$, $k_b d = 0.025$, and $k_b h = 0.325$. According to (3.9), for class III Bragg resonance, we set incident wavenumber $k = 2.031k_b$, and anticipate the resonant generation of a super-harmonic transmitted wave (travelling in the same direction as the incident wave) of wavenumber $k_t \approx 5.062k_b$.

Figure 13 shows the spatial variation of the class III super-harmonic transmitted wave amplitude $A_t(x)$ obtained using HOS with $M = 3$ and $M = 4$ compared with the perturbation solution (4.23) which gives

$$A_t(x) \approx 6.3862(kA)^2(k_b d)(x + L_0/2), \quad -L_0/2 < x < L_0/2. \tag{6.8}$$

The agreement is again excellent for the smaller incident wave steepness $kA = 0.03$, and is acceptable for $kA = 0.06$ for which the perturbation solution still somewhat overestimates A_t.

Note that as indicated by the perturbation solution ((6.7) and (6.8)), the amplitudes of both sub-harmonic reflected and super-harmonic transmitted waves associated with the class III Bragg resonance increase linearly with the width of the bottom patch (L_0) and the bottom slope ($k_b d$) and are quadratic in the incident wave steepness (kA). This behaviour of the solution is confirmed by direct HOS simulations.

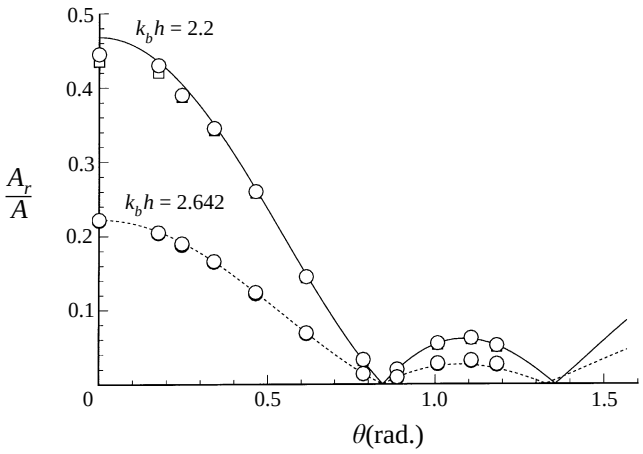

FIGURE 14. Class III sub-harmonic Bragg reflection coefficient as a function of incidence wave angle θ relative to the bottom ripples, for $kA = 0.03$, $k_b d = 0.25$ and $L_0/\lambda_b = 36$. Results plotted are: regular perturbation solutions (——) for $k_b h = 2.2$ and (- - -) for $k_b h = 2.642$; and HOS computations for $M = 3$ (□) and $M = 4$(◯) for the respective mean depths.

6.3.2. *Oblique incidence*

Condition (3.9) indicates that class III Bragg resonance can also occur when the incident wave ($\boldsymbol{k}$) is oblique to the bottom ripples ($\boldsymbol{k}_b$). For this case, a main concern is the influence of the incident angle θ between $\boldsymbol{k}$ and $\boldsymbol{k}_b$ (measured counter-clockwise from $\boldsymbol{k}_b$ say) upon the development and amplitudes of the class III resonant reflected/transmitted double-frequency waves ($\boldsymbol{k}_r$ and $\boldsymbol{k}_t$).

To illustrate oblique sub-harmonic wave reflection under class III Bragg conditions, we employ the same bottom patch as in the normal-incidence reflection case in §6.3.1: $L_0 = 36\lambda_b$, $k_b d = 0.25$, $k_b h = 2.642$. We fix the incident wave steepness to be $kA = 0.03$ and vary the incident angle θ. For a given angle θ, we determine the resonant incident wavenumber magnitude k according to the class III Bragg condition (3.9) and perform a (three-dimensional) HOS simulation to obtain the reflected sub-harmonic wave. Figure 14 shows the comparison between the HOS simulation predictions ($M = 3$ and 4) and the regular perturbation solution (cf. (4.23)) for the class III sub-harmonic reflection coefficient for a wide range of θ. For comparison, the results for a different mean water depth $k_b h = 2.2$ are also shown. The agreement between HOS and perturbation results is excellent. From figure 14, it is seen that the reflected resonant wave amplitude can depend strongly on the mean depth which determines the resonant incident wavenumber via (3.9). Note also the presence of two critical incidence angles at which the propagation of the incident wave is unaffected by the presence of the bottom ripples. The vanishing of the Bragg resonant wave can be seen from (4.23) wherein the terms associated with $\mathscr{B}_2^{(3)}$ and $\mathscr{F}^{(3)}$ cancel exactly at the critical angles.

Class III super-harmonic Bragg transmission can be illustrated in a similar way. We use the same bottom topography as in the normal-incidence transmission case in §6.3.1: $L_0 = 5\lambda_b$ and $k_b d = 0.025$; and, for comparison, again consider two mean water depths $k_b h = 0.25$ and $k_b h = 0.325$. The incident wave steepness is fixed at $kA = 0.03$ and the incident wavenumber k leading to super-harmonic Bragg transmission is obtained from (3.9) for each value of the incidence angle θ over a broad range.

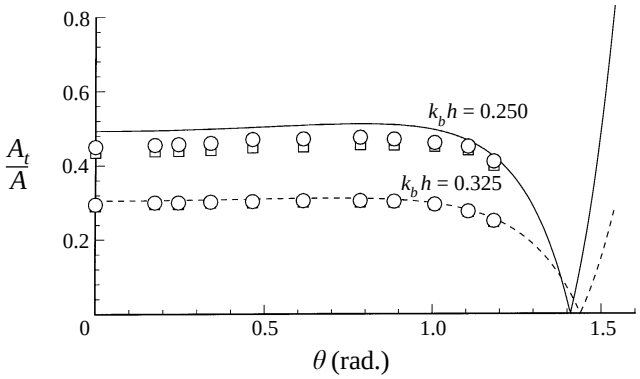

FIGURE 15. Class III Bragg super-harmonic transmission coefficient as a function of incidence wave angle θ relative to the bottom ripples, for $kA = 0.03$, $k_b d = 0.025$ and $L_0/\lambda_b = 5$. Results plotted are: regular perturbation solutions (——) for $k_b h = 0.25$ and (- - -) for $k_b h = 0.325$; and HOS computations for $M = 3$ (□) and $M = 4$ (◯) for the respective mean depths.

Figure 15 plots the (three-dimensional) HOS simulation results and the perturbation solutions (cf. (4.23)) for the transmitted super-harmonic wave amplitude as a function of the incidence angle θ. The HOS and perturbation results again compare well. Unlike the sub-harmonic reflection case above, there exists now only one critical incidence angle at which the resonant class III transmitted wave amplitude vanishes. Below this critical angle the transmitted wave amplitude remains fairly constant for varying θ.

7. Conclusions

We study the generalized Bragg scattering of surface waves by periodic bottom ripples. By considering the general conditions for resonance of the wave–bottom interactions, we obtain, in addition to the known class I and class II Bragg reflections at second- and third-order respectively, conditions for a new third-order class III Bragg resonance. As with class II resonance, the class III Bragg mechanism is also a quartet resonant interaction but involves three surface and one bottom wave components and hence is a manifestation of free-surface nonlinearity. For theoretical guidance, we work out the regular perturbation solutions for these resonances which are relevant for the (initial) spatial/temporal growth of the Bragg resonant waves.

To obtain direct numerical support of the above and to provide a practical solution method for general nonlinear resonant wave–bottom interaction problems, we develop a highly accurate (exponential convergence with number of free-surface and bottom wave modes N) and efficient (computational effort approximately linearly proportional to N) numerical method based on the high-order spectral (HOS) approach of Dommermuth & Yue (1987) and Liu *et al.* (1992) for nonlinear wave–wave and wave–body problems. The method is efficacious for (arbitrary) high-order (M) wave–bottom calculations in two- and three-dimensions and provides a capability for practical wave–bottom interaction computations not available from numerical methods using direct discretizations of the fluid volume or boundary. For illustration, results for M up to 4 in two and three dimensions are presented.

First, we obtain results for normal and oblique incidences over parallel bottom bars under class I and class II (sub-harmonic) Bragg resonance conditions for which there

exist experimental and theoretical (multiple-scale perturbation analysis) results. The agreement is excellent. We then apply the spectral method to the new cases of class II reflection by bi-directional bottom undulations, and class III Bragg resonance. For the realistic values of free-surface and bottom slopes and bottom patch sizes we consider, the amplitudes of the Bragg resonated waves for the third-order (class II and class III) cases can be comparable in magnitude to second-order class I Bragg reflection and the incident wave. Thus, these generalized higher-order Bragg mechanisms may play an appreciable role in the development of nearshore surface waves.

This work is supported financially by grants from the Office of Naval Research (Mechanics & Energy Conversion Division) whose sponsorship is gratefully acknowledged.

Appendix. Calculation of the reflection and transmission coefficients

For a general nonlinear wave field, $\eta(\boldsymbol{x},t)$, composed of incident, $\eta_i(\boldsymbol{x},t)$, reflected, $\eta_r(\boldsymbol{x},t)$, and transmitted, $\eta_t(\boldsymbol{x},t)$, waves, we extend the approach of Goda & Suzuki (1976) to decompose them and thus obtain the reflection and transmission coefficients.

After factoring out the fast spatial and temporal dependences, we can write the free-surface elevation as

$$\eta(\boldsymbol{x},t) = a_r(\boldsymbol{x})\cos(\boldsymbol{k}_r\cdot\boldsymbol{x}-\omega t+\delta_r)+a_t(\boldsymbol{x})\cos(\boldsymbol{k}_t\cdot\boldsymbol{x}-\omega t+\delta_t)+\text{higher harmonics}, \quad (A\,1)$$

where respectively $\boldsymbol{k}_r$ and $\boldsymbol{k}_t$ represent the wavenumbers of the reflected and transmitted waves, a_r and a_t the corresponding wave amplitudes, and δ_r and δ_t their initial phases. It should be noted that the wave amplitudes $a_r(\boldsymbol{x})$ and $a_t(\boldsymbol{x})$ vary only slowly in space $\boldsymbol{x}$. Through a time-harmonic analysis, $\eta(\boldsymbol{x},t)$ also can be expressed as

$$\eta(\boldsymbol{x},t) = \eta_c(\boldsymbol{x})\cos\omega t + \eta_s(\boldsymbol{x})\sin\omega t + \text{higher harmonics}, \quad (A\,2)$$

where the amplitudes, $\eta_c(\boldsymbol{x})$ and $\eta_s(\boldsymbol{x})$, have fast dependences on $\boldsymbol{x}$. At the first harmonic, it follows from (A 1) and (A 2) that

$$a_r(\boldsymbol{x})\cos(\boldsymbol{k}_r\cdot\boldsymbol{x}-\omega t+\epsilon_r)+a_t(\boldsymbol{x})\cos(\boldsymbol{k}_t\cdot\boldsymbol{x}-\omega t+\epsilon_t) = \eta_c(\boldsymbol{x})\cos\omega t+\eta_s(\boldsymbol{x})\sin\omega t. \quad (A\,3)$$

Applying (A 3) at two discrete points ($\boldsymbol{x}$ and $\boldsymbol{x}+\Delta\boldsymbol{x}$) and solving for a_r and a_t, we obtain:

$$a_r(\boldsymbol{x}) = [2-2\cos(\psi_1-\psi_2)]^{-1/2}\left[(\eta_{c2}-\eta_{c1}\cos\psi_2+\eta_{s1}\sin\psi_2)^2 + (\eta_{s2}-\eta_{s1}\cos\psi_2-\eta_{c1}\sin\psi_2)^2\right]^{1/2} \quad (A\,4)$$

and

$$a_t(\boldsymbol{x}) = [2-2\cos(\psi_1-\psi_2)]^{-\frac{1}{2}}\left[(\eta_{c2}-\eta_{c1}\cos\psi_1+\eta_{s1}\sin\psi_1)^2 + (\eta_{s2}-\eta_{s1}\cos\psi_1-\eta_{c1}\sin\psi_1)^2\right]^{1/2} \quad (A\,5)$$

where $\psi_1 = \boldsymbol{k}_r\cdot\Delta\boldsymbol{x}$, $\psi_2 = \boldsymbol{k}_t\cdot\Delta\boldsymbol{x}$, $\eta_{c1} = \eta_c(\boldsymbol{x})$, $\eta_{c2} = \eta_c(\boldsymbol{x}+\Delta\boldsymbol{x})$, $\eta_{s1} = \eta_s(\boldsymbol{x})$, and $\eta_{s2} = \eta_s(\boldsymbol{x}+\Delta\boldsymbol{x})$. The reflection and transmission coefficients are given by $R(\boldsymbol{x}) = a_r(\boldsymbol{x})/a_1$ and $T(\boldsymbol{x}) = a_t(\boldsymbol{x})/a_1$ where a_1 is the first-harmonic amplitude of the incident wave.

We remark that due to the use of the approximation $a_{r,t}(\boldsymbol{x}) \approx a_{r,t}(\boldsymbol{x}+\Delta\boldsymbol{x})$ in obtaining (A 4) and (A 5), small $\Delta\boldsymbol{x}$ (i.e. $|\Delta\boldsymbol{x}| \ll 1$) should be used in practice to obtain high accuracy for a_r and a_t. The above procedure can also be applied to determine the transmission and reflection of other harmonic waves.

REFERENCES

Dalrymple, R. A. & Kirby, J. T. 1986 Water waves over ripples. *J. Waterways, Port, Coastal Ocean Engng* **112**, 309–319.

Davies, A. G. 1982 The reflection of wave energy by undulations on the seabed. *Dyn. Atmos. Oceans* **6**, 207–232.

Davies, A. G. & Heathershaw, A. D. 1984 Surface-wave propagation over sinusoidally varying topography. *J. Fluid Mech.* **144**, 419–443.

Dommermuth, D. G. & Yue, D. K. P. 1987 A high-order spectral method for the study of nonlinear gravity waves. *J. Fluid Mech.* **184**, 267–288.

Goda, Y. & Suzuki, Y. 1976 Estimation of incident and reflected waves in random wave experiments. *Proc. 15th Coastal Engng Conference, Honolulu, Hawaii,* pp. 828–845.

Guazzelli, E., Rey, V. & Belzons, M. 1992 Higher-order Bragg reflection of gravity surface waves by periodic beds. *J. Fluid Mech.* **245**, 301–317.

Heathershaw, A. D. & Davies, A. G. 1985 Resonant wave reflection by transverse bedforms and its relation to beaches and offshore bars. *Mar. Geol.* **62**, 321–338.

Kirby, J. T. 1986 A general wave equation for waves over rippled beds. *J. Fluid Mech.* **162**, 171–186.

Liu, Y. 1994 Nonlinear wave interactions with submerged obstacles with or without current. PhD thesis, Department of Ocean Engineering, Massachusetts Institute of Technology, USA.

Liu, Y., Dommermuth, D. G. & Yue, D. K. P. 1992 A high-order spectral method for nonlinear wave–body interactions. *J. Fluid Mech.* **245**, 115–136.

Mei, C. C. 1985 Resonant reflection of surface water waves by periodic sand-bars. *J. Fluid Mech.* **152**, 315–335.

Mei, C. C., Hara, T. & Naciri, M. 1988 Note on Bragg scattering of water waves by parallel bars on the seabed. *J. Fluid Mech.* **186**, 147–162.

Miles, J. W. 1967 Surface scattering matrix for a shelf. *J. Fluid Mech.* **28**, 755–767.

O'Hare, T. J. & Davies, A. G. 1993 A comparison of two models for surface-wave propagation over rapidly varying topography. *Appl. Ocean Res.* **15**, 1–11.

Phillips, O. M. 1960 On the dynamics of unsteady gravity waves of finite amplitude. Part 1. *J. Fluid Mech.* **9**, 193–217.

Rey, V., Guazzelli, E. & Mei, C. C. 1996 Resonant reflection of surface gravity waves by one-dimensional doubly sinusoidal beds. *Phys. Fluids* **8**, 1525–1530.

Schwartz, L. W. 1974 Computer extension and analytic continuation of Stokes' expansion for gravity waves. *J. Fluid Mech.* **62**, 553–578.

Zakharov, V. E. 1968 Stability of periodic waves of finite amplitude on the surface of a deep fluid. *J. Appl. Mech. Tech. Phys.* **9**, 190–194 (English transl.).